Cellular/Molecular

Deficiency of Cullin 3, a Protein Encoded by a Schizophrenia and Autism Risk Gene, Impairs Behaviors by Enhancing the Excitability of Ventral Tegmental Area (VTA) DA Neurons

Nannan Gao,[1*] Zhipeng Liu,[1*] Hongsheng Wang,[1*] Chen Shen,[1] Zhaoqi Dong,[1] Wanpeng Cui,[1] Wen-Cheng Xiong,[1,2] and Lin Mei[1,2,3,4]

[1]Department of Neurosciences, School of Medicine, Case Western Reserve University, Cleveland, Ohio 44106, [2]Louis Stokes Cleveland Veterans Affairs Medical Center, Cleveland, Ohio 44106, [3]Chinese Institutes for Medical Research, Beijing, China 100069, and [4]Capital Medical University, Beijing, China 100069

The dopaminergic neuromodulator system is fundamental to brain functions. Abnormal dopamine (DA) pathway is implicated in psychiatric disorders, including schizophrenia (SZ) and autism spectrum disorder (ASD). Mutations in Cullin 3 (CUL3), a core component of the Cullin-RING ubiquitin E3 ligase complex, have been associated with SZ and ASD. However, little is known about the function and mechanism of CUL3 in the DA system. Here, we show that CUL3 is critical for the function of DA neurons and DA-relevant behaviors in male mice. CUL3-deficient mice exhibited hyperactive locomotion, deficits in working memory and sensorimotor gating, and increased sensitivity to psychostimulants. In addition, enhanced DA signaling and elevated excitability of the VTA DA neurons were observed in CUL3-deficient animals. Behavioral impairments were attenuated by dopamine D2 receptor antagonist haloperidol and chemogenetic inhibition of DA neurons. Furthermore, we identified HCN2, a hyperpolarization-activated and cyclic nucleotide-gated channel, as a potential target of CUL3 in DA neurons. Our study indicates that CUL3 controls DA neuronal activity by maintaining ion channel homeostasis and provides insight into the role of CUL3 in the pathogenesis of psychiatric disorders.

Key words: **autism spectrum disorder; Cullin3; dopamine; HCN2; neuronal excitability; schizophrenia**

Significance Statement

This study provides evidence that Cullin 3 (CUL3), a core component of the Cullin-RING ubiquitin E3 ligase complex that has been associated with autism spectrum disorder and schizophrenia, controls the excitability of dopamine (DA) neurons in mice. Its DA-specific heterozygous deficiency increased spontaneous locomotion, impaired working memory and sensorimotor gating, and elevated response to psychostimulants. We showed that CUL3 deficiency increased the excitability of VTA DA neurons, and inhibiting D2 receptor or DA neuronal activity attenuated behavioral deficits of CUL3-deficient mice. We found HCN2, a hyperpolarization-activated channel, as a target of CUL3 in DA neurons. Our findings reveal CUL3's role in DA neurons and offer insights into the pathogenic mechanisms of autism spectrum disorder and schizophrenia.

Introduction

Dopamine (DA) is a key neuromodulator involved in motor control, motivation, reward, and cognitive functions (Girault and Greengard, 2004; Pignatelli and Bonci, 2015; Klein et al., 2019). Imbalanced DAergic transmission has been implicated in psychiatric and neurologic conditions. Hyperactive striatal and hypoactive PFC DA systems have been reported in schizophrenia (SZ) (Winterer and Weinberger, 2004; Slifstein et al., 2015; Weinstein et al., 2017). Studies have shown that DA concentrations and DA receptors are significantly increased in the NAc and caudate nucleus of postmortem SZ samples compared with controls (Bird et al., 1979; Mackay et al., 1982). Single-photon computerized emission tomography studies showed higher occupancy of striatal DA D2 receptors (D2DRs) in individuals with SZ, indicating increased synaptic DA concentration (Abi-Dargham et al., 2000). Imbalanced DA signaling has also been implicated in autism spectrum disorder (ASD) (G. M. Anderson, 1994; Pavăl, 2017). Additionally, DA receptor blockers, haloperidol and risperidone, alleviate SZ- and ASD-associated behaviors (L. T. Anderson

Received Feb. 9, 2023; revised July 9, 2023; accepted Aug. 1, 2023.

Author contributions: N.G., Z.L., W.-C.X., and L.M. designed research; N.G., Z.L., H.W., C.S., and Z.D. performed research; N.G., Z.L., and C.S. analyzed data; N.G. wrote the first draft of the paper; N.G., Z.L., and L.M. edited the paper; H.W., Z.D., W.C., and L.M. contributed unpublished reagents/analytic tools.

*N.G., Z.L., and H.W. contributed equally to this work.

This work was supported in part by Case Western Reserve University startup funds to L.M. and W.-C.X. We thank members of the L.M. and W.-C.X. laboratories for critical comments and constructive discussions.

The authors declare no competing financial interests.

Correspondence should be addressed to Lin Mei at lin.mei@case.edu.

https://doi.org/10.1523/JNEUROSCI.0247-23.2023

et al., 1984; Farde et al., 1988; Nyberg et al., 1993; McCracken et al., 2002). Degeneration of DA neurons in the SNc and subsequent decrease in striatal DA levels cause Parkinson's disease (Ehringer and Hornykiewicz, 1960; Barbeau et al., 1962; Kish et al., 1988). The regulation of DA neuronal activity and excitability is complex. Evidence indicates a critical role of hyperpolarization-activated cyclic nucleotide-gated (HCN) channels (Ludwig et al., 1998; Santoro et al., 1998; Okamoto et al., 2006; McDaid et al., 2008; Chu and Zhen, 2010). As homotetramer or heterotetramer voltage-gated ion channels, mammalian HCN channels are encoded by four genes (*Hcn*1-4) and are widely expressed in the nervous system (Santoro et al., 2000; Wahl-Schott and Biel, 2009). HCN2 is the primary subunit in mouse VTA (Notomi and Shigemoto, 2004). Overexpression of HCN2 increases VTA DA neuronal firing (Friedman et al., 2014), whereas knockdown of HCN2 decreases it (Zhong et al., 2017). However, factors affecting the stability of HCN2 in DA neurons remain unclear despite their importance in DA neuronal excitability.

The identification of risk genes for neurologic and psychiatric disorders has significantly advanced our knowledge of the underlying pathologic processes. Cullin 3 (CUL3) is the core component of the Cullin-RING E3 ubiquitin ligase complex (Deshaies, 1999; Pintard et al., 2004). *CUL3* is among the 107 risk genes identified for ASD (De Rubeis et al., 2014), and its variants and mutations have been associated with SZ in several genome-wide association studies (GWASs) (Fromer et al., 2014; Schizophrenia Working Group of the Psychiatric Genomics Consortium, 2014; Greenwood et al., 2019). DA abnormalities associated with SZ and ASD suggest the importance of *CUL3*, an overlapped susceptible gene in both disorders, in DA systems. It has been shown that CUL3-deficient mice displayed anxiety-like behavior, impaired social ability, and dysregulated sensory gating (Dong et al., 2020; Rapanelli et al., 2021, 2023), and CUL3 deficiencies impaired neuronal excitability and synaptic transmission (Escamilla et al., 2017; Kikuma et al., 2019; Dong et al., 2020; Rapanelli et al., 2021, 2023). CUL3 may regulate DA neuronal activity, but its specific function in DA system remains unknown because of the dominant effects of CUL3 deficiency in cell types studied in these mouse models.

Here, we investigated the function of CUL3 in DA system using mice lacking CUL3 selectively in DA neurons. We examined DA-related behaviors and evaluated changes in DA signaling in CUL3-deficient animals. Electrophysiological recordings of VTA DA neurons were performed to explore the underlying mechanisms of abnormal behaviors and DA signaling in CUL3-deficient mice. Pharmacological inhibition of D2DRs and chemogenetic inhibition of DA neurons were conducted to validate the involvement of an overactive DA system in behavioral abnormalities. Furthermore, biochemical analyses were conducted to identify the downstream mechanism for CUL3 deficiency in DA neurons. Our findings reveal a previously unknown function of CUL3 in controlling the excitability of DA neurons and shed light on the pathophysiological mechanisms underlying ASD and SZ.

Materials and Methods

Mice lines and genotyping. DAT::Cre mice (Bäckman et al., 2006), *Cul3*^{flox} mice (McEvoy et al., 2007), and Ai9 mice (Madisen et al., 2010) were described previously and purchased from The Jackson Laboratory (*DAT::Cre*: stock #006660; *Cul3*^{flox}: stock #028349; Ai9: stock #007905). Offspring were screened for the correct genotype by PCR for genomic DNA from the tail. *DAT::Cre* mice were genotyped using primer 1 (5′-TGG CTG TTG GTG TAA AGT GG-3′), primer 2 (5′-GGA CAG GGA CAT GGT TGA CT-3′), and primer 3 (5′-CCA AAA GAC GGC AAT ATG GT-3′). *Cul3*$^{flox/flox}$ mice were genotyped using primer 1 (5′-ATC CCA TCC CAG CAC CCT CTA T-3′), primer 2 (5′-GAA AGG CCA GGT TGT ATT TTA ACT-3′). Ai9 mice were genotyped using primer 1 (5′-AAG GGA GCT GCA GTG GAG TA-3′), primer 2 (5′-CCG AAA ATC TGT GGG AAG TC-3′), primer 3 (5′-GGC ATT AAA GCA GCG TAT CC-3′), and primer 4 (5′-CTG TTC CTG TAC GGC ATG G-3′). Mice were backcrossed into C57BL/6 background (The Jackson Laboratory, stock #000664) and housed in a room with a 12 h light/dark cycle and access to food and water *ad libitum*. P60-P80 male mice were used for behavioral analyses; P30-120 male mice were used for real-time PCR, biochemistry, neuroanatomy, and electrophysiology analyses as described. The Institutional Animal Care and Use Committee of Case Western Reserve University approved all experiments.

Reagents and antibodies. Chemicals were purchased from Sigma-Aldrich unless otherwise indicated. Primary antibodies used were as follows: Phospho-Akt (Thr308) (1:1000 for Western blot; 9275, Cell Signaling Technology); Akt (1:1000 for Western blot; 9272, Cell Signaling Technology); Phospho-TH (Ser40) (1:1000 for Western blot; 2791, Cell Signaling Technology); TH (1:1000 for Western blot, 1:1000 for immunostaining; NB300-109, Novus Biologicals); D2DR (1:250 for Western blot; ADR-002, Alomone Labs); Cullin3 (1:500 for Western blot; A301-109A, Bethyl Laboratories); β-actin (1:5000 for Western blot; ab8226, Abcam); NeuN (1:500 for immunostaining; MAB377, Millipore); HCN1 (1:1000 for Western blot; PA5-78 675, Invitrogen); HCN2 (1:500 for Western blot; PA5-77594, Invitrogen); HCN3 (1:1000 for Western blot; PA5-104434, Invitrogen); HCN4 (1:250 for Western blot; PA5-111878, Invitrogen); Poly-Ubiquitin (1:1000 for Western blot; K63 Linkage, NBP2-36523, Novus Biologicals); and RFP (1:1000 for immunostaining; 600-401-379, Rockland). Secondary antibodies used were as follows: AlexaFluor-488-anti-rabbit IgG (A-11008); AlexaFluor-594-anti-rabbit IgG (A-11012); AlexaFluor-647 anti-mouse IgG (A-21235) antibodies (1:500 for staining) are from Invitrogen; HRP-conjugated goat anti-rabbit IgG (ab205718) and HRP-conjugated goat anti-mouse IgG (ab205719) antibodies (1:5000 for Western blot) are from Abcam. Streptavidin, AlexaFluor-488 conjugate (1:1000 for staining, S32354) is from Invitrogen.

Viruses. All viruses were obtained from Addgene: AAV5-hSyn-DIO-mCherry virus ($\geq 7 \times 10^{12}$ viral genomes/ml, Addgene viral prep #50459-AAV5; RRID:Addgene_50459), AAV5-hSyn-DIO-hM4D (Gi)-mCherry virus ($\geq 7 \times 10^{12}$ viral genomes/ml, Addgene viral prep #44362-AAV5; RRID:Addgene_44362), AAV5-hSyn-DIO-EGFP virus ($\geq 7 \times 10^{12}$ viral genomes/ml, Addgene viral prep #50457-AAV5; RRID:Addgene_50457), and AAV9-rTH-PI-Cre-SV40 virus ($\geq 1 \times 10^{13}$ viral genomes/ml, Addgene viral prep #50457-AAV5; RRID:Addgene_107788).

Behavioral tests. The experimenter was blind to genotypes and treatments during the behavioral tests; mice were recorded using an overhead camera and tracking software (EthoVision, Noldus).

Locomotor activity was measured as described previously (Tan et al., 2018). Mice were placed in a chamber (L × W × H = 50 × 50 × 10 cm) and monitored for movement for 30 min in open field tests or 60 min in cocaine injection experiments.

Rotarod tests were performed as described previously (Dong et al., 2020). In brief, mice were placed onto an accelerated rod after habituation. The rod was accelerated from 4 to 40 rpm within 5 min. The test was performed in three sessions per day, at least 30 min intervals, for 3 consecutive days. The latency to fall was recorded and analyzed.

The Y-maze test was performed as previously described (H. Zhang et al., 2020). A Y-shaped maze with three white, opaque plastic arms at a 120° angle from each other was used. Briefly, mice were placed at the end of one arm of the maze and allowed to freely explore the three arms for 8 min. The total number of arm entries and the number of triads are recorded to calculate the percentage of an alternation. An entry was counted when all four limbs are within the arm. A spontaneous alternation was counted when an animal enters a different arm of the maze in each of three consecutive arm entries. The spontaneous alternation ratio is calculated with the following formula:

$$\text{Spontaneous alternation, \%} = \frac{\textit{number of} \text{ spontaneous alternation}}{\textit{total number of arm entries} - 2} \times 100$$

Prepulse inhibition (PPI) was tested in sound-attenuated chambers (San Diego Instruments) as described previously (Geyer and Swerdlow, 1998). Briefly, mice were placed in a Plexiglas tube connected to a piezoelectric accelerometer for motion detection. Before each test, mice were allowed to habituate to the chamber to 65 dB background white noise for 5 min. During the test, mice were subjected to 12 startle trials (20 ms 120 dB white noise) and 12 prepulse/startle trials (20 ms white noise at 73, 76, or 82 dB, 100 ms intervals, and 20 ms 120 dB white noise). Mouse movement was measured for 100 ms after the startle stimulus onset (sampling frequency 1 kHz). PPI (%) was calculated as follows: 100 × (startle amplitude for pulse alone − startle amplitude for the pulse with prepulse)/startle amplitude for pulse alone.

Western blot. Western blot was performed as previously described (Dong et al., 2020). Briefly, samples were separated by SDS-PAGE, transferred to nitrocellulose membranes, blocked with 5% BSA, probed with specific antibodies, and visualized with enhanced chemiluminescence (32106, Fisher Scientific). Immunoreactive bands were imaged and quantified using the LI-COR Odyssey Fc imaging system (LI-COR Biosciences). To examine the level of specific proteins, tissues were homogenized in modified RIPA buffer [150 mM NaCl, 50 mM Tris-HCl, pH 7.4, 2 mM EDTA, 0.1% SDS, 0.5% Triton X-100, 20% glycerol, 1 mM PMSF, 0.5% sodium deoxycholate, 5 mM NaF, 2 mM Na_3VO_4, and cOmplete protease inhibitor (4693132001, Roche)]. Samples were then centrifuged at 12,000 × *g* for 10 min at 4°C to remove debris. Protein concentration was determined by Pierce BCA Protein Assay Kit (23225, Fisher Scientific), and an equal volume of 2 × SDS sample buffer was added to denature proteins. A total amount of 50 μg proteins was subjected to Western blot. β-actin was used as the loading control.

Ubiquitination assay. The experiment was performed as previously described with minor modifications (Li et al., 2016). VTA/SNc tissues dissected from mice were lysed by sonication in buffer containing 2% SDS, 150 mM NaCl, 10 mM Tris-HCl, pH 8.0, 1 mM PMSF, 0.5% sodium deoxycholate, 5 mM NaF, 2 mM Na_3VO_4, and cOmplete protease inhibitor. After sonication, samples were diluted by adding 9 vol of the dilution buffer containing 10 mM Tris-HCl, pH 8.0, 150 mM NaCl, 2 mM EDTA, and 1% Triton X-100. Samples were then centrifuged at 12,000 × *g* for 10 min at 4°C to remove debris. Then the supernatants were incubated with respective antibodies overnight at 4°C and then with protein A/G agarose beads (sc-2003, Santa Cruz Biotechnology) for 4 h at 4°C. Beads were then washed 3 times, and an equal volume of 2 × SDS sample buffer was added to elute proteins. Precipitated proteins and 5%-10% total lysates were then subjected to Western blotting.

Real-time PCR. Total RNA was isolated using TRIzol reagent (15596018, Invitrogen), and total cDNA was synthesized using a cDNA synthesis kit (GoScript Reverse Transcription System, A5001, Promega). The real-time PCR was performed with SYBR Green qPCR master mix (204056, QIAGEN) in a 20 μl reaction on StepOnePlus real-time PCR system (Applied Biosystems) according to the supplied manuals. The PCR included an initial step at 95°C for 3 min, followed by 40 cycles of denaturation at 95°C for 15 s, annealing, and extension at 60°C for 60 s. Glyceraldehyde 3-phosphate dehydrogenase (*Gapdh*) was used as an internal control. The primers for individual genes were as follows: *Cul3* (forward: 5′-GAG TTC AGG CAA CAT CTA CAG GC-3′, reverse: 5′-GCA CTT TGG TGT GGC TGA CTG A-3′); *Hcn1* (forward: 5′-CAA ATT CTC CCT CCG CAT GTT-3′, reverse: 5′-TGA AGA ACG TGA TTC CAA CTG G-3′); *Hcn2* (forward: 5′-CCG GCG TCA ACA AGT TCT C-3′, reverse: 5′- TGC CCA CGG GAA TGA TAA TGA-3′); *Hcn3* (forward: 5′-AAG GGC TGA CAC CTA TTG TCG-3′, reverse: 5′-CGA ACA CCA CGA GCC ATG T-3′); *Hcn4* (forward: 5′-TTT CAT CTC CTC CAT CCC TGT C-3′, reverse: 5′-CCT GCC GTC CAT ACC CAA T-3′); and *Gapdh* (forward: 5′-AAG GTC ATC CCA GAG CTG AA-3′, reverse: 5′-CTG CTT CAC CAC CTT CTT GA-3′).

Immunohistochemistry. Immunostaining was performed as described previously. In brief, mice were anesthetized with isoflurane and perfused transcardially with 30 ml PBS and 60 ml 4% PFA. Brains were dissected out and fixed in 4% PFA at 4°C for 3 h and dehydrated by 30% sucrose at 4°C for 48 h. Brains were then embedded in Cryo-Embedding Compound (23-730-571, Fisher Scientific), frozen on dry ice, and sectioned into 40 μm slices using a cryostat (HM550, Fisher Scientific). Sections were washed at room temperature with PBS (10 min for 3 times) and incubated with 0.5% PBST (0.5% Triton X-100 in PBS) for 30 min. Slices were then blocked in blocking buffer (10% donkey serum in 0.5% PBST) at room temperature for 1 h and incubated with primary antibodies in the blocking buffer overnight at 4°C. After washing with PBS, sections were incubated with secondary antibodies at room temperature for 1 h. In some experiments, sections were incubated with DAPI to stain nuclei. Finally, slices were washed with PBS and mounted in VECTASHIELD mounting medium (H-1700, Vector Laboratories) and covered with coverslips. Images were collected with a Zeiss confocal laser-scanning microscope (LSM 700).

Nissl staining. Brain sections were mounted onto slides and air-dried in the dark. The sections were then rinsed in deionized water for 5 min, and stained in 0.1% cresyl violet solution for 5-10 min. The sections were sequentially dehydrated in 70%, 80%, and 90% ethanol for 1 min for each concentration. After that, the sections were dehydrated in 100% ethanol for 2 min and cleared with xylene (5 min for 3 times). Last, the sections were mounted with DPX Mountant for Histology (44581, Sigma-Aldrich) and covered with coverslips.

Electrophysiological recording. Horizontal slices (250-μm-thick) containing VTA and SNc were cut from 30-d-old transgenic mice in which DA neurons were labeled with tdTomato as previously described (T. A. Zhang et al., 2010). Briefly, mice were anesthetized and decapitated, the brain was quickly dissected out, and slices were cut with vibratome in ice-cold, oxygenated cutting solution (in mM as follows: NaCl, 120; $NaHCO_3$, 25; KCl, 3.3; NaH_2PO_4, 1.23; $MgSO_4$, 2.4; $CaCl_2$, 1.2; dextrose, 10). Then slices were then incubated at 32°C in the oxygenated cutting solution for 20 min and recovered at room temperature (25°C) in the oxygenated ACSF (in mM as follows: NaCl, 120; $NaHCO_3$, 25; KCl, 3.3; NaH_2PO_4, 1.23; $MgSO_4$, 0.9; $CaCl_2$, 2; dextrose, 10) for at least 1 h, slices were used within 5 h. Slices were transferred to a recording chamber and continuously perfused with oxygenated ACSF. Recording pipettes were made from borosilicate glass (TW150F-4, WPI, 1.5-2.2 MΩ) and filled with intracellular solution (in mM as follows: KCl, 120; EGTA, 0.2; HEPES,10; $MgCl_2$, 2; 280-290 mOsm, pH 7.2 with KOH in DNase-free and RNase-free water). Midbrain neurons were visualized under Nomarski optics (ZeissY), and recordings were made from both tdTomato-labeled neurons within the VTA. The lateral VTA was identified as medial to the medial terminal nucleus of the accessory optic tract (MT) and lateral and rostral to the crest of the medial lemniscus. Cells were voltage-clamped at −60 mV after the break-in, then switched to current-clamp mode to record neuron firing with a current step protocol (−300 to −500 pA in 50 pA steps, 2 s duration). Recordings were then switched back to the voltage-clamp mode, and the cell was again held at −60 mV. I_h was recorded with a voltage step protocol (−40 to −120 mV in 10 mV steps, 1.5 s duration). All calculations of the peak I_h amplitude were taken from a −60 to −120 mV hyperpolarizing step. For current-clamp mode, recordings were digitized at 20 kHz and filtered at 10 kHz; for voltage-clamp mode, recordings were digitized at 10 kHz and filtered at 1 kHz.

Stereotaxic injection. P60 mice were injected with AAV5-hSyn-DIO-mCherry or AAV5-hSyn-DIO-hM4D(Gi)-mCherry viruses, followed by validation and behavioral tests 6 weeks later. P90 mice were injected with AAV5-hSyn-DIO-EGFP or AAV9-rTH-PI-Cre-SV40 virus, followed by validation and behavioral tests 4 weeks later. Mice were anesthetized with ketamine (100 mg/kg) and xylazine (10 mg/kg) and secured in a stereotaxic apparatus (Kopf Instruments). Glass pipette was lowered into the VTA (anteroposterior: −3.0 mm, ML: ± 0.58 mm, and DV: −4.45 mm), and viruses (titer > 10^{12} particles/ml, 200 nl for each side) were injected into at a rate of 10 nl/min. Pipettes were left in place for 5 min before being slowly withdrawn. Injection sites were validated in each mouse after endpoint experiments.

Experimental design and statistical analysis. All data were generated by at least three replicates from independently prepared samples, and the sample size (*n*), and the total number of mice or tissues used per

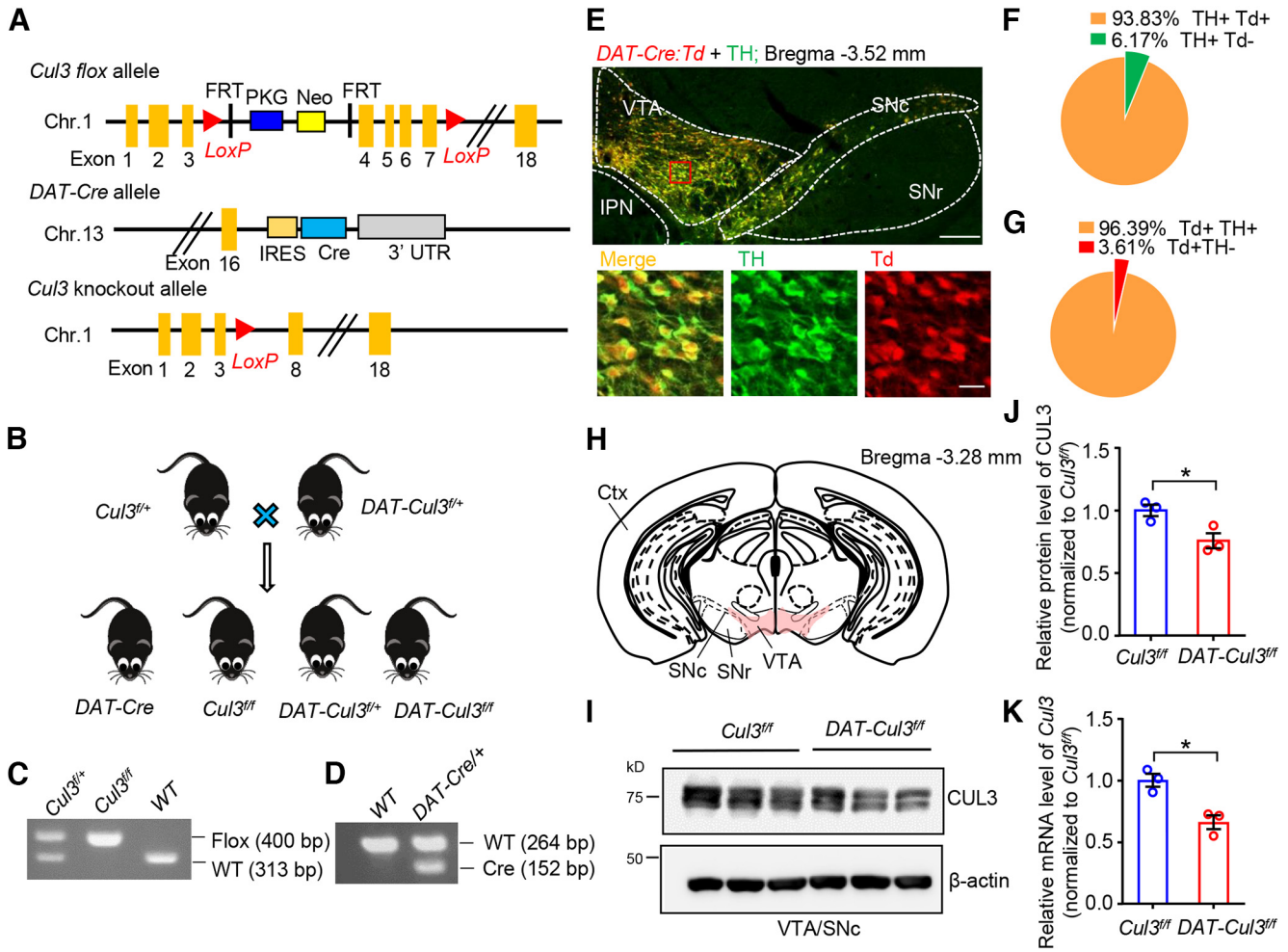

Figure 1. Generation and characterization of *DAT-Cul3* conditional KO mice. ***A***, Schematic diagram of the genomic structure of *Cul3 flox*, *DAT-Cre*, and *Cul3* KO alleles in mice. Chr., chromosome. FRT, flippase recognition target. IRES, internal ribosome entry site. *LoxP*, locus of X-over of P1. Neo, neomycin phosphotransferase gene. PKG, phosphoglycerate kinase I promoter. UTR, untranslated region. ***B***, Genetic strategy for ablation of *Cul3* in DA neurons. $Cul3^{f/+}$ mice were crossed with *DAT::Cre::*$Cul3^{f/+}$ (referred to as *DAT-*$Cul3^{f/+}$) to get *DAT-*$Cul3^{f/f}$ mice together with other indicated genotypes. ***C***, ***D***, Representative PCR genotyping results for *Cul3* allele (***C***) and *DAT-Cre* allele (***D***). ***E***, Representative images of mice midbrain from *DAT::Cre::Ai9* (*DAT-Cre:Td*) mouse at P60. The coronal section of the midbrain was stained with TH (visualized by AlexaFluor-488, green). tdTomato (Td) signals were imaged without further staining. Scale bar, 200 μm. Bottom, Higher magnification of the inset. Scale bar, 20 μm. The Td signals driven by DAT-Cre were restricted to TH-positive DA neurons. IPN, interpeduncular nucleus. ***F***, Ratio of Td/TH double-positive (Td^+ TH^+) in TH^+ neurons in VTA/SNc. ***G***, Ratio of Td/TH double-positive (Td^+ TH^+) in Td^+ neurons in VTA/SNc. ***H***, Schematic diagram of dissecting VTA and part of SNc (VTA/SNc, in pink) on coronal sections for Western blot and real-time PCR assays. Ctx, Cortex; SNr, substantia nigra pars reticulata. ***I***, Reduced CUL3 protein in VTA/SNc in CUL3-deficient mice at P60. Homogenates of VTA/SNc were subjected to Western blotting. ***J***, Quantification for data in ***I***. $n = 3$ mice per group; $Cul3^{f/f}$ versus *DAT-*$Cul3^{f/f}$, $p = 0.0375$, $t_{(3.709)} = 3.175$; unpaied *t* test. ***K***, Reduced mRNA levels of *Cul3* determined by real-time PCR for VTA/SNc in *DAT-*$Cul3^{f/f}$ mice compared with $Cul3^{f/f}$ controls at P60. $n = 3$ mice per group; $Cul3^{f/f}$ versus *DAT-*$Cul3^{f/f}$, $p = 0.0118$, $t_{(3.981)} = 4.403$; unpaied *t* test. Data are mean ± SEM. *$p < 0.05$.

group were provided in the figure legends. Data were analyzed by unpaired *t* test, one-way ANOVA (with Tukey's *post hoc* test), and two-way ANOVA (with Bonferroni's *post hoc* test). GraphPad Prism (version 7, GraphPad Software) was used for statistical analysis. Data are shown as mean ± SEM. Statistical difference was considered when $p < 0.05$.

Results

Generation of conditional CUL3-deficient mice

To investigate the physiological role of the *Cul3* gene and the consequences of its disruption in the DA system, we bred $Cul3^{flox/flox}$ ($Cul3^{f/f}$) mice (McEvoy et al., 2007) with a *DAT::Cre*-expressing mouse line (*DAT-Cre*) to generate DA neuron-specific heterozygous and homozygous deletions of *Cul3* (*DAT-*$Cul3^{f/+}$ mice and *DAT-*$Cul3^{f/f}$ mice, respectively) (Fig. 1*A-D*). In *DAT-Cre* mice, Cre recombinase is expressed under the control of endogenous DA transporter (DAT), a protein specifically expressed in DA neurons (Bäckman et al., 2006) (Fig. 1*A*). *DAT-Cre* mice were further crossed with *Ai-9* mice (Madisen et al., 2010) to generate offspring in which the Cre-driven-tdTomato (Td) will be expressed in DAT-positive neurons. Similar to a previous report (Lammel et al., 2015), the DAT-Cre-driven Td is detected in the majority (93.8%) of TH-positive (TH^+) DA neurons and also limited to TH^+ DA neurons (96.4%) (Fig. 1*E-G*). These results demonstrate the specificity of *DAT-Cre* mouse line used in this study. Furthermore, *DAT-Cre* and $Cul3^{f/f}$ mice were used as controls to demonstrate that the observed phenotype is because of the loss of *Cul3*. We verified reduced protein levels of CUL3 in the VTA/SNc region (Fig. 1*H*) of *DAT-*$Cul3^{f/f}$ mouse by Western blot (Fig. 1*I,J*) and reduced mRNA levels of *Cul3* using real-time PCR (Fig. 1*K*).

Constitutive homozygous deletion or disruption of the *Cul3* gene is embryonic lethal (Singer et al., 1999; Amar et al., 2021). Homozygous deletion of *Cul3* in cortical pyramidal neurons was reported to cause decreased body size, atrophy and disrupted lamination in cortical regions, and premature death (Rapanelli et al., 2021; Dong et al., 2020; Morandell et al., 2021). These observations indicate that CUL3 is necessary for neuronal survival and

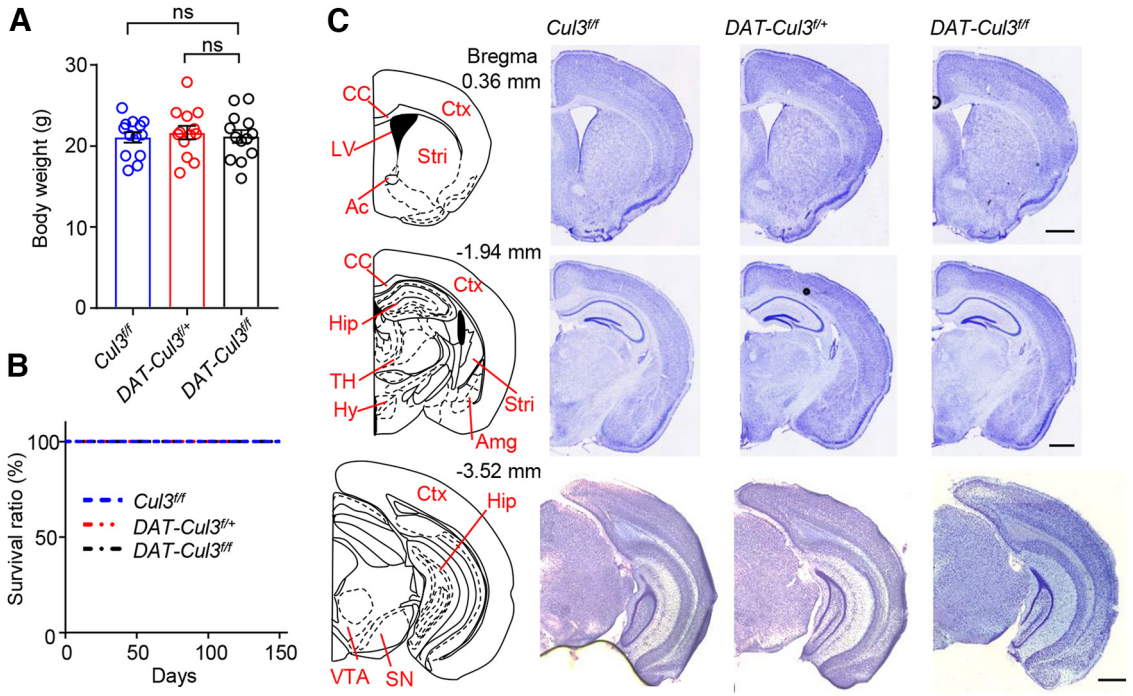

Figure 2. Intact gross neuroanatomy in adult *DAT-Cul3*$^{f/+}$ and *DAT-Cul3*$^{f/f}$ mice. ***A***, Comparable body weights for mice of indicated genotypes at P60. Data are mean ± SEM. $n = 13$ mice per group; *Cul3*$^{f/f}$ versus *DAT-Cul3*$^{f/+}$, $p = 0.8520$; *Cul3*$^{f/f}$ versus *DAT-Cul3*$^{f/f}$, $p = 0.9958$; $F_{(2,36)} = 0.1683$; one-way ANOVA followed by Tukey's *post hoc* test. ***B***, Similar survival ratio for mice of indicated genotypes. $n = 13$ mice per group. ***C***, Similar gross morphology of brain sections from indicated genotypes at P60. Shown are representative images for Nissl staining of coronal sections at bregma 0.36 mm, −1.94 mm, and −3.52 mm. Scale bar, 200 μm. Ac, Anterior commissure; Amg, amygdala; CC, corpus callosum; Ctx, cortex; Hip, hippocampus; Hy, hypothalamus; LV, lateral ventricle; SN, substantia nigra; Stri, striatum; TH, thalamus. Scale bar, 1 mm. Data are mean ± SEM.

development and promote us to examine general neuroanatomy and survival of DA neurons in CUL3-deficient animals (Figs. 2, 3). Both heterozygous and homozygous KO mice were viable and fertile, they displayed similar body weights and survived as long as the *Cul3*$^{f/f}$ mice (Fig. 2*A*,*B*). Nissl staining of brain slices from adult animals revealed that there were no significant differences in the gross brain anatomy among animals from three genotypes, indicating that CUL3 deficiency in DA neurons did not disrupt general brain development (Fig. 2*C*).

Reduced survival of midbrain DA neurons in CUL3-deficient mice

To study the impact of CUL3 deficiency on DA neuron development, brain tissues were isolated from mice at three different ages and subjected to immunohistochemistry analyses. Brain slices containing the VTA/SNc region were stained using antibodies against TH and NeuN. DA neurons were visualized by Td, whose expression is driven by Cre and costained with anti-TH antibodies (Fig. 3). The numbers of TH-positive (TH$^+$) cells in the VTA/SNc region were similar among three different genotypes: controls (*DAT-Cre*), *DAT-Cul3*$^{f/+}$, and *DAT-Cul3*$^{f/f}$ at P30 (Fig. 3*A*,*D*). However, beginning at P60, the number of TH$^+$ cells in *DAT-Cul3*$^{f/f}$ mice was decreased compared with controls (*DAT-Cre*) (Fig. 3*B*,*C*,*F*,*H*), indicating a necessary role of CUL3 for DA neuron development. To further investigate this, we quantified Td-labeled neurons that are positive for NeuN (i.e., Td$^+$ NeuN$^+$). As shown in Fig. 3*A*, *E*, the numbers of Td$^+$ NeuN$^+$ cells in the VTA/SNc region were comparable among controls (*DAT-Cre*), *DAT-Cul3*$^{f/+}$, and *DAT-Cul3*$^{f/f}$ at P30. Consistently, starting at P60, fewer Td$^+$ NeuN$^+$ cells were detected in *DAT-Cul3*$^{f/f}$ mice but not *DAT-Cul3*$^{f/+}$ mice compared with controls (*DAT-Cre*) (Fig. 3*B*, *C*,*G*,*I*). At P120, the numbers of Td$^+$ NeuN$^+$ cells were further reduced in *DAT-Cul3*$^{f/f}$ mice but not *DAT-Cul3*$^{f/+}$ mice. Because the reduction was not observed in P30 *DAT-Cul3*$^{f/f}$ or *DAT-Cul3*$^{f/+}$ mice, these results suggest a problematic survival of DA neurons in the absence of CUL3 and reveal a role of the protein in DA neuron development. DA neurons were comparable between control mice and heterozygous CUL3-deficient (*DAT-Cul3*$^{f/+}$) mice; therefore, the latter were used in subsequent investigations.

DA-related behavioral deficits in CUL3-deficient mice

To investigate whether CUL3 deficiency impacts the function of DA neurons, we assessed *DAT-Cul3*$^{f/+}$ mice in a range of DA-related tasks, including locomotor activity, spatial working memory, sensorimotor gating, and psychostimulant sensitivity. To assess their spontaneous, novelty-induced motor activities, *DAT-Cre*, *Cul3*$^{f/f}$, and *DAT-Cul3*$^{f/+}$ mice (8-week-old) were subjected to the open field test (Fig. 4*A*-*C*). We found that *DAT-Cul3*$^{f/+}$ mice were more active (Fig. 4*A*) and traveled longer distances than controls (*DAT-Cre* and *Cul3*$^{f/f}$ mice) during the observed period (Fig. 4*B*), indicating hyperactive locomotion in CUL3-deficient animals. Next, anxiety-like behavior was evaluated by measuring the time mice spent exploring the central area of the arena (Fig. 4*C*). *DAT-Cul3*$^{f/+}$ mice spent similar time in the central area, compared with controls, suggesting that CUL3 deficiency did not significantly change the anxiety level in mice. Meanwhile, we did not detect significant differences regarding these measurements between *DAT-Cre* and *Cul3*$^{f/f}$ mice. These results indicate that the *Cul3* deficiency in DA neurons causes locomotion hyperactivity, a sign of an overactive DA system.

Y-maze tests were conducted to evaluate spatial working memory, a behavior impacted by DA function (Fig. 4*D*-*F*). We found that the spontaneous alternation ratio decreased in *DAT-Cul3*$^{f/+}$ mice compared with *DAT-Cre* or *Cul3*$^{f/f}$ mice (Fig. 4*E*),

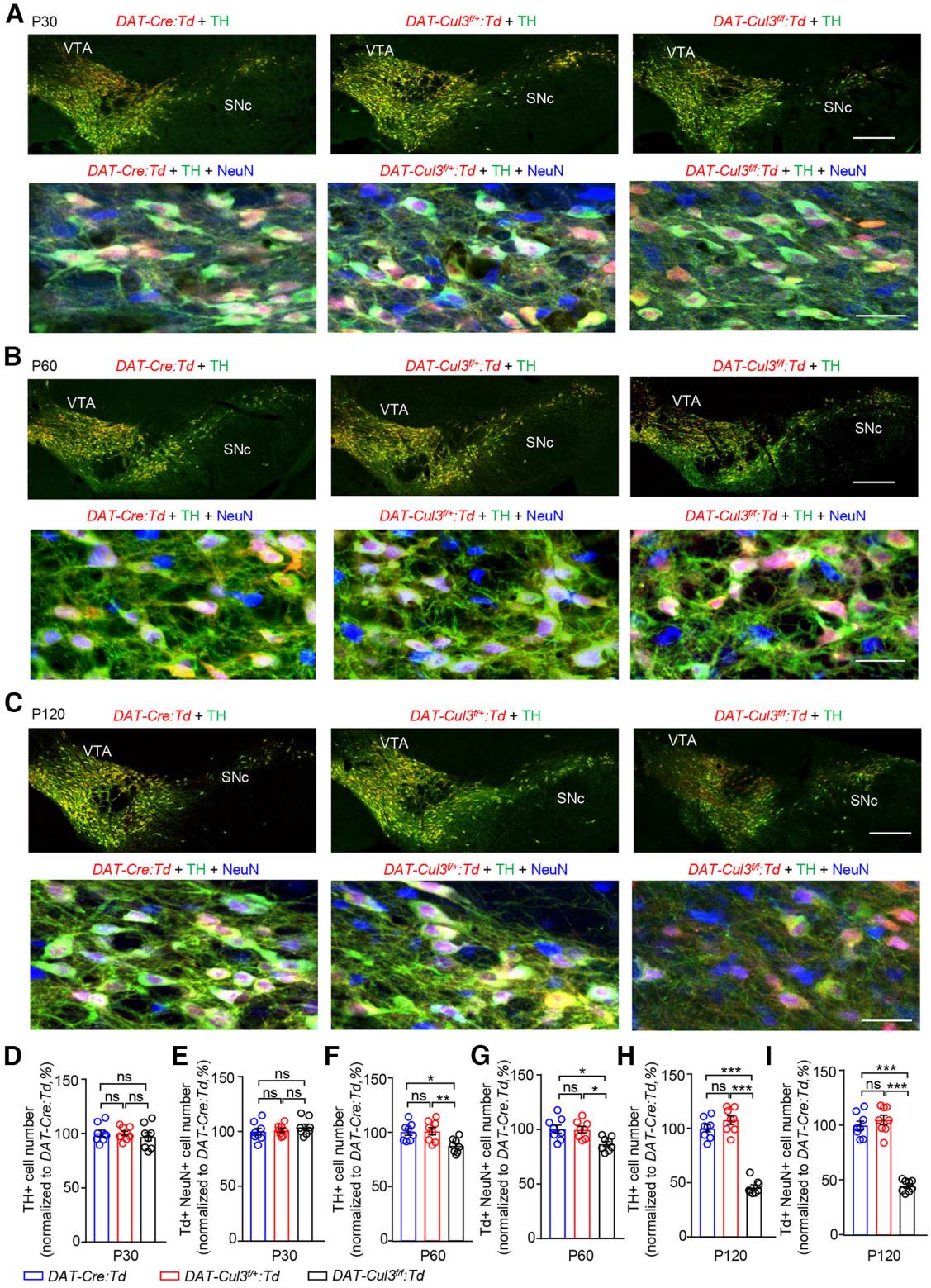

Figure 3. Comparable numbers of midbrain DA neurons in adult *DAT-Cul3*$^{f/+}$ mice. ***A***, Similar number of midbrain DA neurons in P30 *DAT-Cul3*$^{f/+}$*:Td* and *DAT-Cul3*$^{f/f}$*:Td* mice compared with controls (*DAT-Cre:Td*). Top, Representative images for VTA/SNc in coronal sections of the midbrain at bregma −3.5 mm. Sections were stained with TH antibodies (green) and imaged directly for the Td (red) signal. Scale bar, 200 μm. Bottom, Enlarged images of VTA for indicated genotypes. Coronal sections were stained with TH (green) and NeuN (blue) antibodies, and Td (red) signals were imaged without further staining. Scale bar, 20 μm. ***B***, Decreased VTA/SNc DA neurons in P60 *DAT-Cul3*$^{f/f}$*:Td* mice, but not *DAT-Cul3*$^{f/+}$*:Td* mice, compared with controls (*DAT-Cre:Td*). Top, Representative images for VTA/SNc in coronal sections of the midbrain at bregma −3.53 mm. Sections were stained with TH antibodies (green) and imaged directly for the tdTomato (Td, red) signal. Scale bar, 200 μm. Bottom, Enlarged images of VTA for indicated genotypes. Coronal sections were stained with TH (green) and NeuN (blue) antibodies, and Td (red) signals were imaged without further staining. Scale bar, 20 μm. ***C***, Decreased VTA/SNc DA neurons in P120 *DAT-Cul3*$^{f/f}$*:Td* mice, but not *DAT-Cul3*$^{f/+}$*:Td* mice, compared with controls (*DAT-Cre:Td*). Top, Representative images for VTA/SNc in coronal sections of the midbrain at bregma −3.5 mm. Sections were stained with TH antibodies (green) and imaged directly for the tdTomato (Td, red) signal. Scale bar, 200 μm. Bottom, Enlarged images of VTA for indicated genotypes. Coronal sections were stained with TH (green) and NeuN (blue) antibodies, and Td (red) signals were imaged without further staining. Scale bar, 20 μm. ***D***, ***E***, Similar number of TH$^+$ (***D***) and Td$^+$ NeuN$^+$ cells (***E***) in VTA/SNc of *DAT-Cul3*$^{f/f}$*:Td* and *DAT-Cul3*$^{f/+}$*:Td* mice compared with controls

while it did not differ between the two control groups (*DAT-Cre* vs *Cul3*$^{f/f}$ mice). Furthermore, the total number of arm entries was similar among the three genotypes (Fig. 4*F*). These data indicate an impaired working memory in CUL3-deficient mice. Additionally, the Rotarod test was performed to assess motor performance, especially motor coordination (Fig. 4*G*). The latency to fall was similar among *DAT-Cul3*$^{f/+}$, *DAT-Cre*, and *Cul3*$^{f/f}$ mice, indicating that CUL3 deficiency did not impact general motor function. This unaffected motor function implies that the impaired working memory function observed in CUL3-deficient animals was not because of motor coordination deficits. DA was reported to exhibit an inverted U-shaped impact on working memory (Cools and D'Esposito, 2011); thus, the impacted working memory suggests an imbalanced DA signaling in *DAT-Cul3*$^{f/+}$ mice. Furthermore, PPI test was performed to determine whether the sensorimotor gating function is affected by CUL3 deficiency in DA neurons (Fig. 4*H-J*). PPI refers to the reduction in startle response produced by a weaker prepulse stimulus (Hoffman and Ison, 1980; Geyer et al., 1990) (Fig. 4*H*) and is a reliable measure of sensorimotor gating reflex across species (Swerdlow et al., 2016). *DAT-Cul3*$^{f/+}$ mice exhibited similar amplitudes of acoustic startle in responses to *DAT-Cre* and *Cul3*$^{f/f}$ mice (Fig. 4*I*), suggesting normal hearing and acoustic startle reflex. However, the PPI ratio was notably lower in CUL3-deficient animals compared with controls (Fig. 4*J*). In addition, there was no difference in the PPI between *DAT-Cre* and *Cul3*$^{f/f}$ mice. Reduced PPI has also been associated with increased striatal DA in rodents (Swerdlow et al., 1990a, 1992), and therefore impaired sensorimotor gating function in CUL3-deficient mice could imply increased DA signaling.

In *DAT-Cul3*$^{f/+}$ mice, CUL3 was deleted in DA neurons not only in VTA, but also in other brain regions, such as dorsal raphe nucleus and subregions of the hypothalamus. To further study CUL3 in VTA DA neurons, we sought to delete *Cul3* in DA neurons specifically in the VTA by injecting AAV9-rTH-PI-Cre-SV40 (AAV9-TH-Cre) virus into the VTA of adult *Cul3*$^{f/+}$ mice (Fig. 5*A*). AAV9-TH-Cre expresses Cre under the control of a rat TH promoter (Addgene_107788, James M. Wilson, unpublished data) that has been shown to direct the expression of Cre in TH$^+$ neurons (Parker et al., 2019; Vandegrift et al., 2020). Western blot results indicated that, 4 weeks after viral injection, CUL3 was reduced in the VTA of AAV9-TH-Cre-injected *Cul3*$^{f/+}$ mice compared with controls (injected with AAV5-hSyn-DIO-GFP or AAV5-DIO-GFP for short) (Fig. 5*B*,*C*). AAV9-TH-Cre-injected *Cul3*$^{f/+}$ mice displayed similar phenotypes of *DAT-Cul3*$^{f/+}$ mice, such as increased locomotion in the open field (Fig. 5*D-F*) and decreased PPI (Fig. 5*I*,*J*). These results demonstrate that CUL3 in VTA DA neurons is necessary for proper DA-related behaviors.

Finally, we examined whether cocaine-induced hyperlocomotion was impacted by *Cul3* deficiency. Mice were habituated to an open area before being injected with saline (vehicle, veh) or cocaine (10 mg/kg, i.p., arrow). As shown in Figure 6, *DAT-Cul3*$^{f/+}$ mice are more active than *Cul3*$^{f/f}$ mice when treated with vehicle (*DAT-Cul3*$^{f/+}$ + veh vs *Cul3*$^{f/f}$ + veh) (Fig. 6*A*,*B*), which is consistent with the data from the open field test (Fig. 4*B*). Moreover, cocaine increased the total distance traveled by *Cul3*$^{f/f}$ and *DAT-Cul3*$^{f/+}$ mice by 2.8- and 3.5-fold, respectively (Fig. 6*B*). These data indicate that both genotypes responded to cocaine, but *DAT-Cul3*$^{f/+}$ mice exhibit greater responses in locomotor activity. Increased sensitivity to psychostimulants, such as cocaine, has been associated with increased striatal DA transmission in mice (Bello et al., 2011). Furthermore, in line with the aforementioned findings, these data also suggest enhanced DA signaling in *DAT-Cul3*$^{f/+}$ mice.

Increased DA signaling in CUL3-deficient mice

To determine whether enhanced DA signaling may serve as a pathologic mechanism, we focused on the NAc of the striatum, a key downstream brain region that receives projections from VTA DA neurons (Fig. 7*A*). DA functions through binding to D1 or D2 receptors (D1DRs or D2DRs; G-protein-coupled receptors) (Missale et al., 1998; Neve et al., 2004; Tritsch and Sabatini, 2012). D2DR is a key target of antipsychotics to inhibit DA transmission (Seeman et al., 1975; Meltzer et al., 1989). Decreased levels of phospho-TH at Ser40 (pTH Ser40) have been correlated with the activity of presynaptic D2DR (Anzalone et al., 2012), and reduced phospho-Akt at Thr308 (pAkt Thr308) reflects the activity of postsynaptic D2 signaling (Beaulieu et al., 2007). Notably, pTH Ser40 and pAkt Thr308 levels were lower in the CUL3-deficient NAc than those in controls (Fig. 7*B*,*C*). There was no apparent change in protein levels of D2DR or Akt. These findings suggest increased DA signaling in NAc of the CUL3-deficient mice.

Next, we investigated whether behavioral abnormalities in CUL3-deficient mice could be ameliorated by D2 antagonist haloperidol (Fig. 7*D-G*). Mice were treated with haloperidol (0.8 mg/kg, i.p.) or veh 30 min before behavioral tests. As shown in Figure 7*D*, *DAT-Cul3*$^{f/+}$ mice injected with haloperidol showed reduced locomotor activities compared with vehicle-treated mice, and time spent in the central area of the open field is not changed (Fig. 7*E*). In addition, the PPI ratio in haloperidol-treated *DAT-Cul3*$^{f/+}$ mice improved compared with vehicle-treated *DAT-Cul3*$^{f/+}$ mice (Fig. 7*F*), while acoustic startle amplitude remained unchanged (Fig. 7*G*), indicating that haloperidol attenuated the loss of PPI in CUL3-deficiency animals without affecting their startle response. These findings revealed that reducing DA signaling reversed the behavioral deficits observed in animals lacking CUL3, implying that the behavioral deficits observed in CUL3-deficient animals may be caused by an increase in DA signaling.

A critical role of CUL3 in the excitability of VTA DA neurons

To investigate how CUL3 deficiency causes increased DA activity, we first evaluated whether there are any changes in the structural characteristics of VTA DA neurons in *DAT-Cul3*$^{f/+}$mice. Immunostaining assays were performed to examine DA

←

(*DAT-Cre:Td*) at P30. $n = 8$ slices from 4 mice per genotype. ***E***, *DAT-Cul3*$^{f/+}$*:Td* versus *DAT-Cre:Td*, $p > 0.9999$; *DAT-Cul3*$^{f/f:}$ *Td* versus *DAT-Cre:Td*, $p = 0.7605$; *DAT-Cul3*$^{f/f:}$ *Td* versus *DAT-Cul3*$^{f/+}$*:Td*, $p = 0.7670$; $F_{(2,21)} = 0.3306$. ***F***, *DAT-Cul3*$^{f/+}$*:Td* versus *DAT-Cre:Td*, $p = 0.9455$; *DAT-Cul3*$^{f/f:}$ *Td* versus *DAT-Cre:Td*, $p = 0.5173$; *DAT-Cul3*$^{f/f:}$ *Td* versus *DAT-Cul3*$^{f/+}$*:Td*, $p = 0.7113$; $F_{(2,21)} = 0.6559$. ***F***, ***G***, Reduced number of TH$^+$ (***F***) and Td$^+$ NeuN$^+$ cells (***G***) in VTA/SNc of *DAT-Cul3*$^{f/f}$*:Td* mice, but not *DAT-Cul3*$^{f/+}$*:Td* mice compared with control (*DAT-Cre:Td*) at P60. $n = 8$ slices from 4 mice per genotype. ***G***, *DAT-Cul3*$^{f/+}$*:Td* versus *DAT-Cre:Td*, $p = 0.9785$; *DAT-Cul3*$^{f/f:}$ *Td* versus *DAT-Cre:Td*, $p = 0.0149$; *DAT-Cul3*$^{f/f:}$ *Td* versus *DAT-Cul3*$^{f/+}$*:Td*, $p = 0.0095$; $F_{(2,21)} = 6.78$. ***H***, *DAT-Cul3*$^{f/+}$*:Td* versus *DAT-Cre:Td*, $p = 0.9916$; *DAT-Cul3*$^{f/f:}$ *Td* versus *DAT-Cre:Td*, $p = 0.0102$; *DAT-Cul3*$^{f/f:}$ *Td* versus *DAT-Cul3*$^{f/+}$*:Td*, $p = 0.0135$; $F_{(2,21)} = 6.788$. ***H***, ***I***, Reduced number of TH$^+$ (***H***) and Td$^+$ NeuN$^+$ cells (***I***) in VTA/SNc of *DAT-Cul3*$^{f/f:}$ *Td* mice, but not *DAT-Cul3*$^{f/+}$*:Td* mice compared with control (*DAT-Cre:Td*) at P120. $n = 8$ brain slices from 4 mice per genotype. ***I***, *DAT-Cul3*$^{f/+}$*:Td* versus *DAT-Cre:Td*, $p = 0.2569$; *DAT-Cul3*$^{f/f:}$ *Td* versus *DAT-Cre:Td*, $p < 0.0001$; *DAT-Cul3*$^{f/f:}$ *Td* versus *DAT-Cul3*$^{f/+}$*:Td*, $p < 0.0001$; $F_{(2,21)} = 113.2$. ***J***, *DAT-Cul3*$^{f/+}$*:Td* versus *DAT-Cre:Td*, $p = 0.5695$; *DAT-Cul3*$^{f/f:}$ *Td* versus *DAT-Cre:Td*, $p < 0.0001$; *DAT-Cul3*$^{f/f:}$ *Td* versus *DAT-Cul3*$^{f/+}$*:Td*, $p < 0.0001$; $F_{(2,21)} = 98.19$; one-way ANOVA followed by Tukey's *post hoc* test. Data are mean ± SEM. $^*p < 0.05$. $^{**}p < 0.01$. $^{***}p < 0.001$.

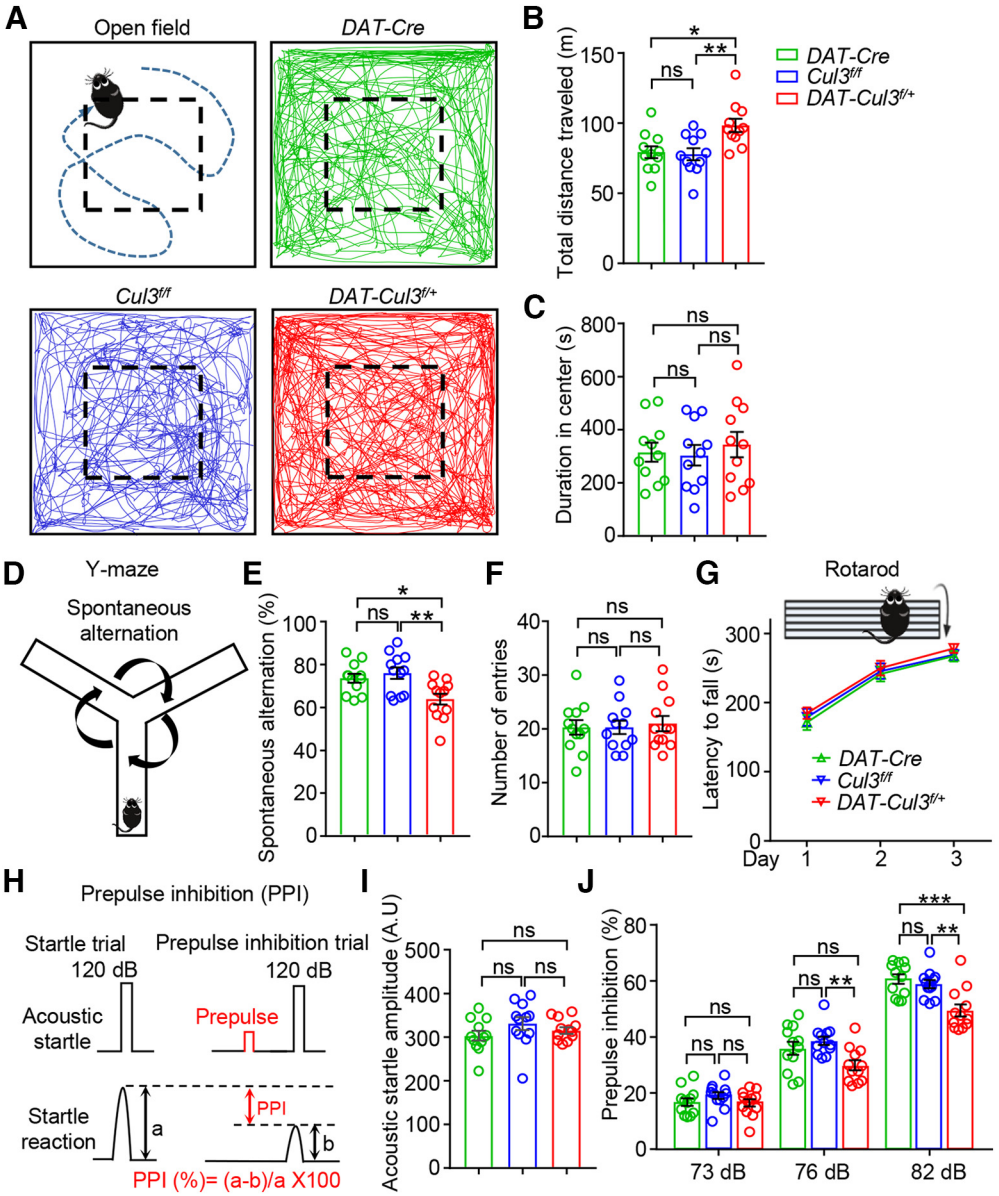

Figure 4. Increased locomotion, impaired working memory, and decreased sensorimotor gating in *DAT-Cul3*$^{f/+}$ mice. ***A***, Schematic diagram of the open field test and representative traces of movement over 30 min in the arena (50 × 50 × 20 cm) for mice of indicated genotypes. ***B***, Increased distance traveled by *DAT-Cul3*$^{f/+}$ mice compared with *DAT-Cre* mice or *Cul3*$^{f/f}$ mice. $n = 11$ mice per group; *DAT-Cre* versus *Cul3*$^{f/f}$, $p = 0.9709$; *DAT-Cre* versus *DAT-Cul3*$^{f/+}$, $p = 0.0117$; *Cul3*$^{f/f}$ versus *DAT-Cul3*$^{f/+}$, $p = 0.0065$; $F_{(2,30)} = 6.871$; one-way ANOVA followed by Tukey's *post hoc* test. ***C***, Similar time spent in the central area of the open field by *DAT-Cul3*$^{f/+}$ mice. $n = 11$ mice per group; *DAT-Cre* versus *Cul3*$^{f/f}$, $p = 0.9797$; *DAT-Cre* versus *DAT-Cul3*$^{f/+}$, $p = 0.8652$; *Cul3*$^{f/f}$ versus *DAT-Cul3*$^{f/+}$, $p = 0.7613$; $F_{(2,30)} = 0.267$; one-way ANOVA followed by Tukey's *post hoc* test. ***D***, Schematic diagram of the Y-maze test. Spontaneous alternation behavior is shown as the mouse's tendency to explore a new arm of the maze instead of returning to one that was previously visited. ***E***, Decreased spontaneous alternation in Y-maze test by *DAT-Cul3*$^{f/+}$ mice. $n = 12$ mice per group; *DAT-Cre* versus *Cul3*$^{f/f}$, $p = 0.7781$; *DAT-Cre* versus *DAT-Cul3*$^{f/+}$, $p = 0.0218$; *Cul3*$^{f/f}$ versus *DAT-Cul3*$^{f/+}$, $p = 0.0039$; $F_{(2,33)} = 6.847$; one-way ANOVA followed by Tukey's *post hoc* test. ***F***, Similar total number of entries in Y-maze test. $n = 12$ mice per group; *Cre* versus *Cul3*$^{f/f}$, $p > 0.9999$; *DAT-Cre* versus *DAT-Cul3*$^{f/+}$, $p = 0.9159$; *Cul3*$^{f/f}$ versus *DAT-Cul3*$^{f/+}$, $p = 0.9159$; $F_{(2,33)} = 0.1066$; one-way ANOVA followed by Tukey's *post hoc* test. ***G***, Comparable latency to fall in the Rotarod test. $n = 13$ mice per group; $p = 0.3742$, $F_{(genotype)(2108)} = 0.9919$; two-way ANOVA. ***H***, Schematic diagram of PPI experiment. PPI (%) $= (a - b)/a \times 100$. ***I***, Similar acoustic startle reflex. $n = 12$ mice per group; *Cre* versus *Cul3*$^{f/f}$, $p = 0.2185$; *DAT-Cre* versus *DAT-Cul3*$^{f/+}$, $p = 0.7511$; *Cul3*$^{f/f}$ versus *DAT-Cul3*$^{f/+}$, $p = 0.5940$; $F_{(2,33)} = 1.464$; one-way ANOVA followed by Tukey's *post hoc* test. ***J***, Decreased PPI ratio at 76 and 82 dB in *DAT-Cul3*$^{f/+}$ mice. $n = 12$ mice per group. At 73 dB, *Cre* versus *Cul3*$^{f/f}$, $p = 0.4345$; *DAT-Cre* versus *DAT-Cul3*$^{f/+}$, $p = 0.9841$; *Cul3*$^{f/f}$ versus *DAT-Cul3*$^{f/+}$, $p = 0.3435$; $F_{(2,33)} = 1.198$. At 76 dB, *Cre* versus *Cul3*$^{f/f}$, $p = 0.5942$; *DAT-Cre* versus *DAT-Cul3*$^{f/+}$, $p = 0.0782$; *Cul3*$^{f/f}$ versus *DAT-Cul3*$^{f/+}$, $p = 0.0078$; $F_{(2,33)} = 5.472$. At 82 dB, *Cre* versus *Cul3*$^{f/f}$, $p = 0.9256$; *DAT-Cre* versus *DAT-Cul3*$^{f/+}$, $p = 0.0010$; *Cul3*$^{f/f}$ versus *DAT-Cul3*$^{f/+}$, $p = 0.0027$; $F_{(2,33)} = 9.765$; one-way ANOVA followed by Tukey's *post hoc* test. Data are mean ± SEM. $^*p < 0.05$. $^{**}p < 0.01$. $^{***}p < 0.001$.

projections. Axonal arborization of DA neurons in P60 mice was examined by TH staining in the NAc and mPFC, two major efferent target regions of the VTA DA neurons (Fig. 8). The intensity of TH immunostaining of the DA terminals in NAc (Fig. 8*A-C*) or mPFC (Fig. 8*D-G*) did not change in *DAT-Cul3*$^{f/+}$ mice. Next, we examined the dendritic morphology of VTA DA neurons by injecting biocytin into *Td*-positive neurons in brain slices of *DAT-Cre:Td* and *DAT-Cul3*$^{f/+}$*:Td* mice followed by *post hoc* staining (Fig. 8*H*). The dendritic length (Fig. 8*I*) and the complexity of the dendrite (Fig. 8*J*) of the putative VTA DA neurons were similar between *DAT-Cul3*$^{f/+}$ and control slices. Together, these observations suggest that CUL3 deficiency did not interrupt the neuroanatomy of the DA pathway in mice at the time of the experiment.

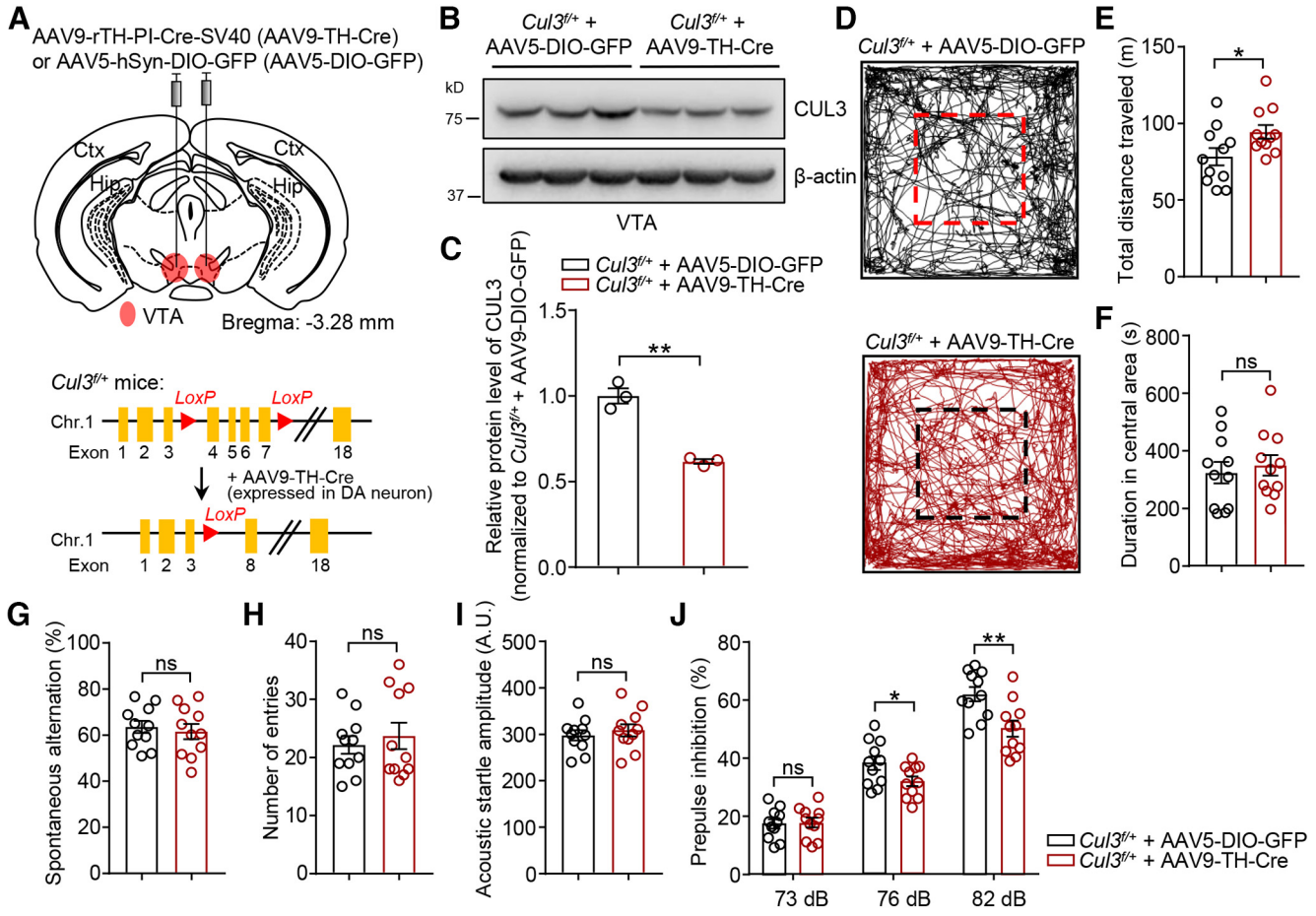

Figure 5. Increased locomotion and decreased sensorimotor gating induced by VTA DA neuron-specific *Cul3* deficiency. ***A***, Schematic diagram represents injection of AAV9-rTH-Cre (AAV9-TH-Cre) virus into VTA in P90 $Cul3^{f/+}$ mouse (top) and experimental approach for Cre-dependent deletion of *Cul3* in DA neurons (right). AAV5-hSyn-DIO-GFP (AAV5-DIO-GFP) virus was injected as control. ***B***, Reduced CUL3 protein in VTA tissues from $Cul3^{f/+}$ mice injected with AAV9-TH-Cre 4 weeks after injection. ***C***, Quantification for data in ***B***. $n = 3$ mice per group; $p = 0.0087$, $t_{(2.368)} = 8.152$; unpaired *t* test. ***D***, Representative traces of movement over 30 min in the arena for $Cul3^{f/+}$ mice injected with indicated viruses. ***E***, Increased distance traveled by AAV9-TH-Cre-injected $Cul3^{f/+}$ mice in the open field compared with AAV5-DIO-GFP-injected mice. $n = 11$ mice, $p = 0.0376$, $t_{(19.12)} = 2.234$; unpaired *t* test. ***F***, Comparable time spent in the center in the open field. $n = 11$ mice, $p = 0.6361$, $t_{(19.94)} = 0.4805$; unpaired *t* test. ***G***, Similar spontaneous alternation in $Cul3^{f/+}$ mice injected with AAV9-TH-Cre and those with AAV5-DIO-GFP in Y-maze test. $n = 11$ mice, $p = 0.6340$, $t_{(19.24)} = 0.4837$; unpaired *t* test. ***H***, Comparable total number of entries in Y-maze. $n = 11$ mice, $p = 0.5809$, $t_{(17.32)} = 0.5627$; unpaired *t* test. ***I***, Similar acoustic startle reflex. $n = 11$ mice, $p = 0.5301$, $t_{(19.31)} = 0.6394$; unpaired *t* test. ***J***, Impaired PPI at 76 and 82 dB in AAV9-TH-Cre-injected $Cul3^{f/+}$ mice. $n = 11$ mice, $p = 0.8599$, $t_{(19.99)} = 0.1788$ for 73 dB; $p = 0.0451$, $t_{(18.17)} = 2.152$ for 76 dB; $p = 0.0042$, $t_{(19.68)} = 3.234$ for 82 dB; unpaired *t* test. Data are mean ± SEM. $^*p < 0.05$. $^{**}p < 0.01$.

Considering the unchanged morphologic features, we examined whether the electrophysiological properties of VTA DA neurons are altered in *DAT-*$Cul3^{f/+}$ mice. VTA DA neurons were identified as *Td*-positive cells in *DAT-Cre:Td* and *DAT-*$Cul3^{f/+}$*:Td* mice and whole-cell patch-clamp recordings were conducted on acute brain slices (Fig. 9*A*). Current-clamp recordings were performed in the lateral portion of the VTA, where the majority of DA neurons project to the NAc Shell (Lammel et al., 2011). Recorded neurons were later verified by *post hoc* confocal microscopy of injected biocytin and TH staining (Fig. 9*B*). VTA DA neurons in *Cul3*-deficient mice had a higher input resistance than that in control mice (Fig. 9*C*). However, CUL3-deficient neurons showed little changes in the resting membrane potential (Fig. 9*D*) and capacity (Fig. 9*E*) compared with controls. Action potentials (APs) of VTA DA neurons were elicited by injecting depolarizing currents at different intensities. As shown in Figure 9*F*,*G*, the firing frequency of VTA DA neurons in response to somatic current injections was higher in *DAT-*$Cul3^{f/+}$*:Td* mice compared with *DAT-Cre:Td* mice. In *ex vivo* slice preparation, midbrain DA neurons retain the tonic pacemaker firing pattern and exhibit spontaneous single-spike discharge (Grace and Onn, 1989; Lacey et al., 1989). As presented in Figure 9*H*,*I*, the spontaneous firing frequency of the *Cul3*-deficient VTA DA neurons is higher than that of control neurons. Together, these results indicate that *Cul3* deficiency increases the intrinsic excitability of VTA DA neurons.

Alleviating behavioral deficits by chemogenetic inhibition of DA neurons

To further investigate the functional significance of the increased excitability of VTA DA neurons in animals lacking CUL3, we evaluated whether the behavioral phenotypes of *Cul3*-deficient mice could be altered by suppressing neuronal activity. We sought to reduce the activity of VTA DA neurons in adult mice using a DREADDs (designer receptors exclusively activated by designer drugs) chemical genetic approach. *DAT-*$Cul3^{f/+}$ mice were bilaterally injected with AAV5-DIO-hM4D(Gi)-mCherry (hM4Di), which expresses hM4D in a Cre-dependent manner (Fig. 10*A*) (Krashes et al., 2011). hM4D is an M4 muscarinic acetylcholine receptor engineered to inhibit neurons when bound to clozapine N-oxide (CNO) via inhibitory G protein (Gi)-dependent activation of the inward potassium channel (Armbruster et

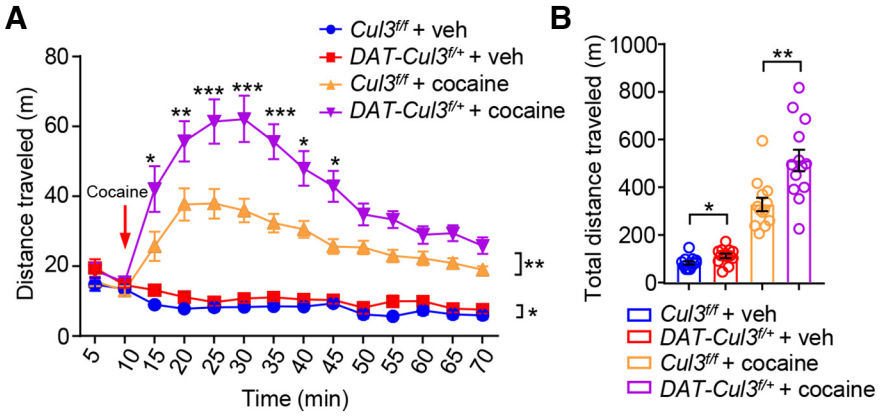

Figure 6. Increased responsiveness to psychostimulant in *DAT-Cul3*$^{f/+}$ mice. ***A***, Increased distance traveled by *DAT-Cul3*$^{f/+}$ mice, shown as 5 min intervals during 10 min before and 60 min after cocaine injection (indicated by a red arrow). $n = 13$ mice per group. *Cul3*$^{f/f}$ + veh versus *DAT-Cul3*$^{f/+}$ + veh, $p = 0.0238$, $F_{(1,24)} = 5.82$; *Cul3*$^{f/f}$ + cocaine versus *DAT-Cul3*$^{f/+}$ + cocaine, $p = 0.0018$, $F_{(1,\ 24)} = 12.37$; two-way ANOVA followed by Bonferroni's *post hoc* test. ***B***, Increased total distance traveled by *DAT-Cul3*$^{f/+}$ mice within 60 min after cocaine injection. $n = 13$ mice per group. *Cul3*$^{f/f}$ + veh versus *DAT-Cul3*$^{f/+}$ + veh, $p = 0.0178$, $t_{(22.18)} = 2.561$; *Cul3*$^{f/f}$ + cocaine versus *DAT-Cul3*$^{f/+}$ + cocaine, $p = 0.0025$, $t_{(19.92)} = 3.454$; unpaired *t* test. Data are mean ± SEM. *$p < 0.05$. **$p < 0.01$. ***$p < 0.001$.

al., 2007; Urban and Roth, 2015). Virus lacking hM4D (AAV5-hSyn-DIO-mCherry, mCherry) was injected as control. *Post hoc* staining confirmed that the injected virus was largely expressed in VTA (Fig. 10*H*). Mice were treated with CNO (2 mg/kg, i.p.) or vehicle (saline) 30 min before behavioral tests (Zhu et al., 2014). Treatment of CNO reduced the total distance traveled by *DAT-Cul3*$^{f/+}$ mice in the open field (Fig. 10*B*) without changing the time spent in the center arena (Fig. 10*C*). CNO injection improved the spontaneous alteration ratio of *DAT-Cul3*$^{f/+}$ mice in the Y-maze (Fig. 10*D*) while not altering the number of entries into arms (Fig. 10*E*). Additionally, the PPI ratio of the *DAT-Cul3*$^{f/+}$ mice increased after CNO injection (Fig. 10*F*), whereas the acoustic startle responses in these animals remain unchanged after CNO treatment (Fig. 10*G*). Our findings suggest that the hyperactivity, working memory deficits, and diminished sensorimotor gating seen in *DAT-Cul3*$^{f/+}$ mice can be alleviated by decreasing the activity of DA neurons in the VTA.

Increased I_h in CUL3-deficient VTA DA neurons

To further investigate the mechanism by which CUL3 controls DA neuron excitability, we analyzed single AP in the trains of VTA DA neuron spontaneous firing (Fig. 11*A*,*B*). We found that the AP threshold (Fig. 11*C*), AP spike amplitude (Fig. 11*D*), and AP half-width (Fig. 11*E*) were comparable between VTA DA neurons from *DAT-Cul3*$^{f/+}$*:Td* and *DAT-Cre:Td* mice. However, the amplitude of afterhyperpolarization potentials (AHPs) notably decreased in *DAT-Cul3*$^{f/+}$ VTA DA neurons compared with controls (Fig. 11*F*,*G*). The interspike intervals were smaller in CUL3-deficient VTA DA neurons than that in controls (Fig. 11*H*), consistent with increased excitability in these neurons. These detailed analyses of AP indicate that CUL3 is necessary for proper AHP amplitude in VTA DA neurons and suggest elevated excitability of CUL3-deficient VTA DA neurons could be a result of decreased AHP.

Hyperpolarization-activated cation current (I_h) mediated by hyperpolarization-activated cyclic nucleotide-gated (HCN) channels plays a key role in regulating the AHP in DA neurons (Neuhoff et al., 2002; McDaid et al., 2008). It has been shown that increasing HCN channel current leads to decreased AHP and elevated AP firing in VTA DA neurons (Chu and Zhen, 2010; Santos-Vera et al., 2013; Friedman et al., 2014). To investigate the involvement of I_h, we performed *ex vivo* electrophysiological recordings of I_h of DA neurons in lateral VTA on brain slices from control and CUL3-deficient mice. As shown in Figure 12*A*, I_h was induced by hyperpolarizing voltage steps (from −60 to −130 mV with 10 mV steps, 1.5 s duration) followed by a step to −130 mV for analysis of tail currents. I_h amplitude was calculated by subtracting the instantaneous current from the steady-state current (Fig. 12*A*, arrows). Voltage-clamp recording showed that the I_h amplitude (Fig. 12*B*) and density (Fig. 12*C*) increased in CUL3-deficient VTA DA neurons compared with control neurons. This change was not likely because of the differences in cell size, since membrane capacitance was not significantly different between control and CUL3-deficient neurons (Fig. 12*D*). Moreover, the application of HCN channel blocker ZD7288 (Harris and Constanti, 1995) abolished the increase in I_h from *DAT-Cul3*$^{f/+}$*:Td* neurons compared with *DAT-Cre:Td* neurons (Fig. 12*E*,*F*), suggesting that the change in I_h was largely because of enhanced HCN channel function. Collectively, these findings imply that CUL3 deficiency increases VTA DA neuron excitability by amplifying the currents of HCN channels.

A necessary role of CUL3 for HCN2 ubiquitination

Functional HCN channels are tetramers that exist in either heteromeric or homomeric compositions (Accili et al., 2002). In mouse VTA, all four HCN subtypes (HCN1-4) are detectable (Monteggia et al., 2000) and HCN2 has been reported as the major HCN subunit (Notomi and Shigemoto, 2004). To determine the HCN subtype(s) that changed in the *DAT-Cul3*$^{f/+}$ mouse, we conducted Western blot to examine the protein levels of HCN1-4 channels in the VTA/SNc regions. As shown in Figure 12*G*,*H*, the protein level of HCN2 was higher in VTA/SNc tissues from P60 *DAT-Cul3*$^{f/+}$ mice than that in *Cul3*$^{f/f}$ mice, whereas there were little changes in the protein levels of HCN1, HCN3, and HCN4. In contrast, mRNA levels of *Hcn1-4* were similar between *DAT-Cul3*$^{f/+}$ and *Cul3*$^{f/f}$ mice (Fig. 12*I*), suggesting post-transcriptional changes caused by CUL3 deficiency. These results support the notion that the increased excitability of CUL3-deficient VTA DA neurons may be mediated by the upregulation of HCN2 channels. Next, we investigated the molecular mechanisms underlying HCN2 protein increase in *DAT-Cul3*$^{f/+}$ mice. As a critical cofactor for the RING complex of ubiquitination E3 ligases, CUL3 might control the ubiquitination

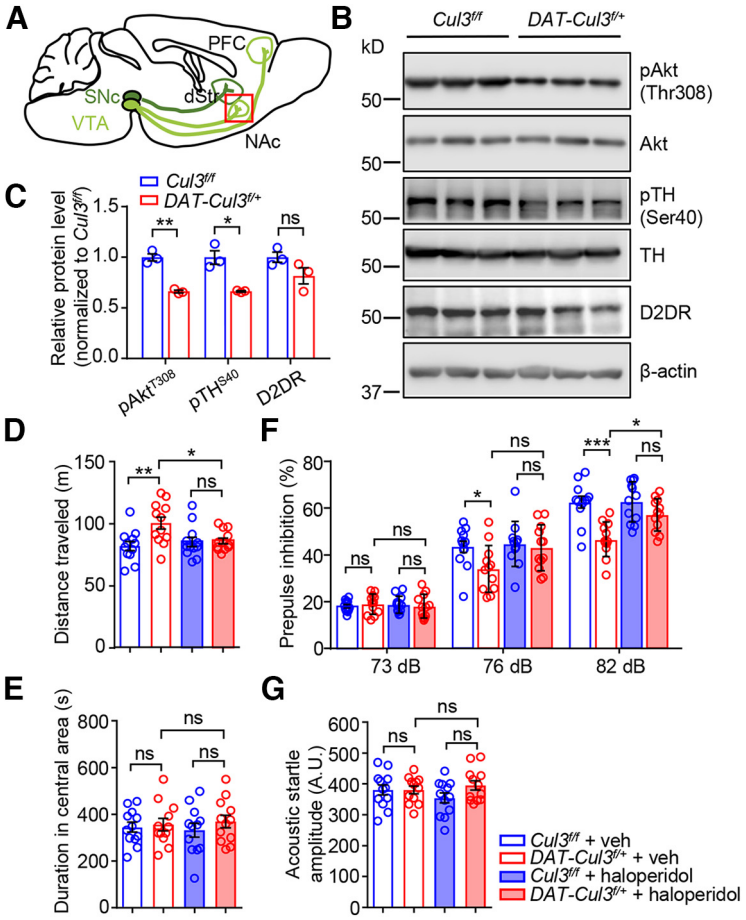

Figure 7. Increased DA signaling in *DAT-Cul3*$^{f/+}$ mice. ***A***, Schematic diagram represents projections of VTA DA neurons (in light green) and SNc DA neurons (in dark green). Red inset represents NAc, showing that this brain region was collected and subjected to experiment in ***B***. dStr, dorsal striatum. ***B***, Reduced levels of pAkr Thr308 and pTH Ser40 in NAc of P60 *DAT-Cul3*$^{f/+}$ mice compared with *Cul3*$^{f/f}$ mice. ***C***, Quantification of data in ***B***. $n = 3$ mice for each genotype; for pAkt, $p = 0.0054$, $t_{(2.585)} = 8.77$; for pTH, $p = 0.0382$, $t_{(2.025)} = 4.906$; for D2DR, $p = 0.1404$, $t_{(3.35)} = 1.924$; unpaired *t* test. ***D***, Haloperidol attenuated hyperlocomotion in *DAT-Cul3*$^{f/+}$ mice. $n = 12$ mice for each group; veh-treated *Cul3*$^{f/f}$ versus veh-treated *DAT-Cul3*$^{f/+}$, $p = 0.0065$; haloperidol-treated *Cul3*$^{f/f}$ versus haloperidol-treated *DAT-Cul3*$^{f/+}$, $p = 0.9986$; veh-treated *DAT-Cul3*$^{f/+}$ versus haloperidol-treated *DAT-Cul3*$^{f/+}$, $p = 0.0473$; $F_{(3,44)} = 4.72$; one-way ANOVA followed by Tukey's *post hoc* test. ***E***, No difference in time spent in the central area of the open field. $n = 12$ mice for each group; veh-treated *Cul3*$^{f/f}$ versus veh-treated *DAT-Cul3*$^{f/+}$, $p = 0.9918$; haloperidol-treated *Cul3*$^{f/f}$ versus haloperidol-treated *DAT-Cul3*$^{f/+}$, $p = 0.7333$; veh-treated *DAT-Cul3*$^{f/+}$ versus haloperidol-treated *DAT-Cul3*$^{f/+}$, $p = 0.9814$; $F_{(3,44)} = 0.3802$; one-way ANOVA followed by Tukey's *post hoc* test. ***F***, Haloperidol restored the PPI ratio in *DAT-Cul3*$^{f/+}$ mice at 82 dB. $n = 12$ mice for each group. For 73 dB, veh-treated *Cul3*$^{f/f}$ versus veh-treated *DAT-Cul3*$^{f/+}$, $p = 0.9520$; haloperidol-treated *Cul3*$^{f/f}$ versus haloperidol-treated *DAT-Cul3*$^{f/+}$, $p = 0.9711$; veh-treated *DAT-Cul3*$^{f/+}$ versus haloperidol-treated *DAT-Cul3*$^{f/+}$, $p = 0.9436$; $F_{(3,44)} = 0.1611$. For 76 dB, veh-treated *Cul3*$^{f/f}$ versus veh-treated *DAT-Cul3*$^{f/+}$, $p = 0.0447$; haloperidol-treated *Cul3*$^{f/f}$ versus haloperidol-treated *DAT-Cul3*$^{f/+}$, $p = 0.1496$; veh-treated *DAT-Cul3*$^{f/+}$ versus haloperidol-treated *DAT-Cul3*$^{f/+}$, $p = 0.6500$; $F_{(3,44)} = 4.55$. For 82 dB, veh-treated *Cul3*$^{f/f}$ versus veh-treated *DAT-Cul3*$^{f/+}$, $p < 0.001$; haloperidol-treated *Cul3*$^{f/f}$ versus haloperidol-treated *DAT-Cul3*$^{f/+}$, $p = 0.3345$; veh-treated *DAT-Cul3*$^{f/+}$ versus haloperidol-treated *DAT-Cul3*$^{f/+}$, $p = 0.0130$; $F_{(3,44)} = 10.58$; one-way ANOVA followed by Tukey's *post hoc* test. ***G***, Similar acoustic startle response. $n = 12$ mice for each group; veh-treated *Cul3*$^{f/f}$ versus veh-treated *DAT-Cul3*$^{f/+}$, $p > 0.9999$; haloperidol-treated *Cul3*$^{f/f}$ versus haloperidol-treated *DAT-Cul3*$^{f/+}$, $p = 0.2531$; veh-treated *DAT-Cul3*$^{f/+}$ versus haloperidol-treated *DAT-Cul3*$^{f/+}$, $p = 0.9088$; $F_{(3,44)} = 1.225$; one-way ANOVA followed by Tukey's *post hoc* test. Data are mean ± SEM. $^{*}p < 0.05$. $^{**}p < 0.01$. $^{***}p < 0.001$.

of HCN2. To test this hypothesis, *in vivo* ubiquitination of HCN2 was examined in *DAT-Cul3*$^{f/+}$ mice and control. HCN2 was immunoprecipitated from VTA/SNc homogenates using anti-HCN2 antibodies and probed with anti-K48-linked-ubiquitin, a specific type of ubiquitination that targets proteins for degradation (Chau et al., 1989). As shown in Figure 12*J*, K48-linked-ubiquitination of HCN2 was reduced in the VTA/SNc tissues from *DAT-Cul3*$^{f/+}$ mice compared with *Cul3*$^{f/f}$ mice. Our findings suggest that CUL3 plays a vital role in the ubiquitination process of HCN2, thereby controlling the protein level of this channel in DA neurons.

Discussion

Here, we investigated the specific role of CUL3 in DA neurons. First, the deficiency of CUL3 in DA neurons impaired DA-related behaviors without severely disrupting the neurogenesis and morphology of DA neurons. Heterozygous CUL3-deficient animals exhibited hyperactive locomotion, impaired working memory performance, sensorimotor gating deficits, and increased response to psychostimulants. Second, enhanced DA signaling and increased intrinsic excitability of VTA DA neurons were found in CUL3-deficient mice. Moreover, hyperactive locomotion and impaired PPI in heterozygous KO animals were ameliorated by blocking D2DRs and inhibiting the activity of DA neurons chemogenetically. These results imply that the behavioral deficits in CUL3-deficient animals are caused by an overactive DA system. Third, we found increased function and protein levels of HCN2, a hyperpolarization-activated channel critical for neuronal excitability, in the midbrain of *DAT-Cul3*$^{f/+}$ mice. These data suggest insufficient ubiquitination of HCN2 as a pathophysiological mechanism of CUL3 deficiency in DA neurons. Together, these results

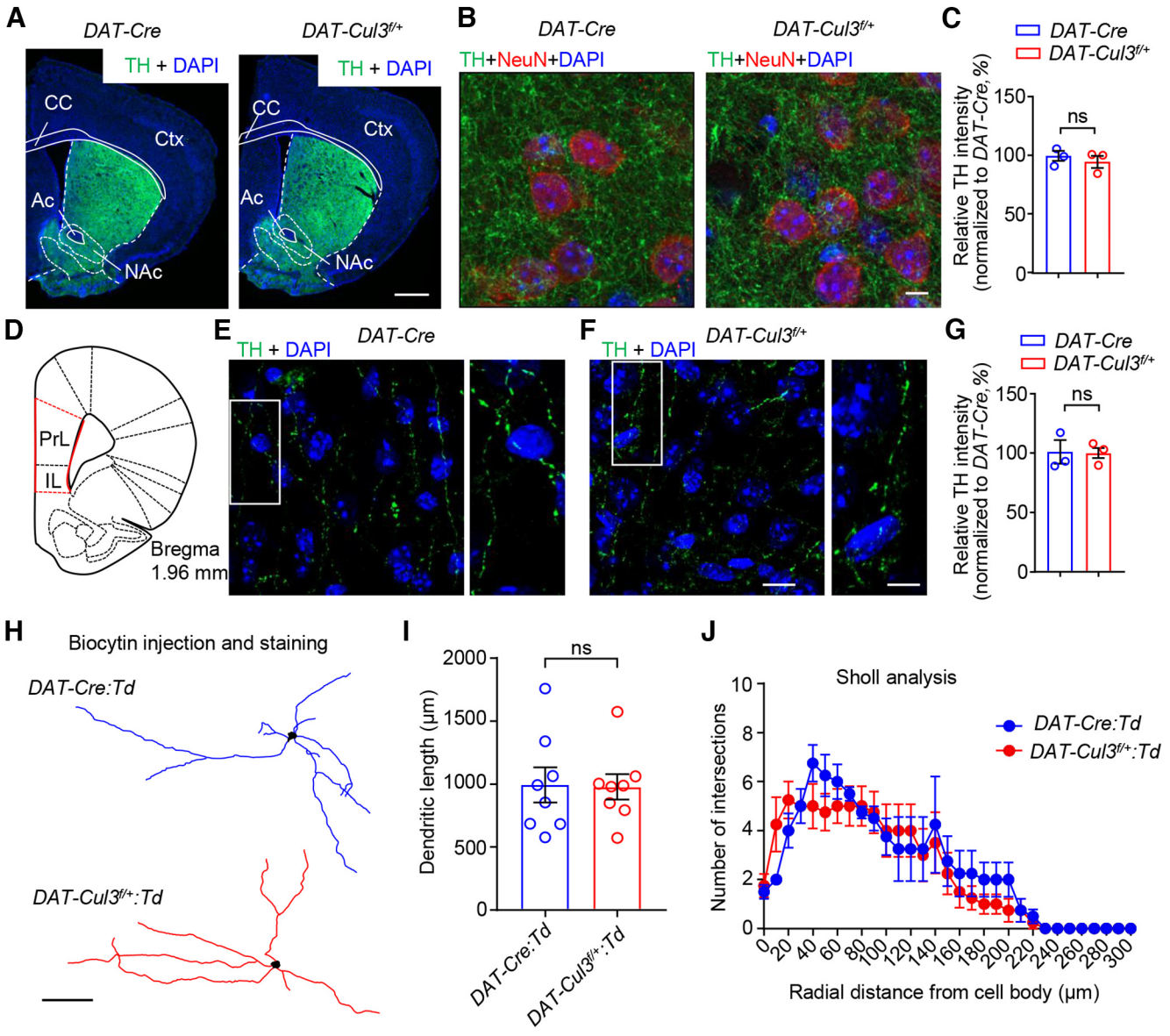

Figure 8. Comparable axon terminals and dendritic morphology of VTA DA neuron in adult *DAT-Cul3*$^{f/+}$ mice. ***A–C***, Comparable morphology and TH intensity in the striatum between P60 *DAT-Cul3*$^{f/+}$ mice and control. The striatum was stained with antibodies toward TH (green), NeuN (red), and DAPI (blue). ***A***, Representative images of striatum from P60 mice. Scale bar, 500 μm. ***B***, Representative images of NAc from control and *DAT-Cul3*$^{f/+}$ mice. Scale bar, 5 μm. ***C***, Quantification of TH intensity in NAc. $n = 3$ mice per genotype with 10 ROIs per mouse. $p = 0.4879$, $t_{(3.836)} = 0.7664$; unpaired t test. Ac, Anterior commissure; CC, corpus callosum; Ctx, cortex. ***D***, Schematic diagram of a coronal section at bregma 1.96 mm indicating the location of mPFC (red lines). PrL, Prelimbic cortex; IL, infralimbic cortex. ***E–G***, No difference in TH intensity in mPFC between adult *DAT-Cul3*$^{f/+}$ mice and control. ***E***, ***F***, Representative images of mPFC from P60 mice. mPFC was stained with TH (green) and DAPI (blue). Right, Enlarged images from the insets. Scale bars: left panels, 10 μm; right panels, 5 μm. ***G***, Quantification of TH intensity in mPFC. $n = 3$ mice per genotype with 10 ROIs per mouse. $p = 0.9320$, $t_{(2.752)} = 0.0934$; unpaired t test. ***H***, Representative reconstruction of VTA DA neurons of P60 *DAT-Cre:Td* and *DAT-Cul3*$^{f/+}$*:Td* mice. DA neurons were labeled with biocytin after whole-cell patch recording in brain slices. Scale bar, 100 μm. ***I***, No difference in total length of dendrites. $n = 8$ neurons of 3 mice per genotype, $p = 0.9250$, $t_{(12.78)} = 0.0960$; unpaired t test. ***J***, Similar complexity of dendrite in control and *DAT-Cul3*$^{f/+}$ mice by Sholl analysis. $n = 8$ neurons of 3 mice per genotype; $p = 0.3362$, $F_{(1186)} = 0.9296$; two-way ANOVA. Data are mean ± SEM.

indicate a critical role of CUL3 in controlling intrinsic neuronal excitability and function of the DA pathways. We recognize that this study focused on male mice and yielded limited insights into the role of CUL3 in female animals, which warrants future research.

A pathway analysis of recent GWAS data showed convergence in DA pathway genes as potential genetic risk factors in individuals with ASD and those with SZ (Khanzada et al., 2017), suggesting dysregulated DA signaling as a common underlying etiology despite different presentations. *Cul3* is identified as a susceptible gene associated with both disorders (De Rubeis et al., 2014; Schizophrenia Working Group of the Psychiatric Genomics Consortium, 2014; Greenwood et al., 2019), suggesting that mutations in CUL3 may contribute to the pathogenesis of ASD and SZ in similar or shared biological processes. CUL3 regulates a variety of cellular functions (Andérica-Romero et al., 2013), including cell cycle (Singer et al., 1999), cell death (Lee et al., 2010), cellular stress response (Kaspar et al., 2009), cytoskeleton organization (Morandell et al., 2021), neuronal neurogenesis (Amar et al., 2021), and morphogenesis (Djagaeva and Doronkin, 2009; Lin et al., 2011). The function of CUL3 in the nervous system has been studied in a neuronal type-specific manner. It has been shown that CUL3 deficiency in pyramidal neurons causes aberrant behaviors, including

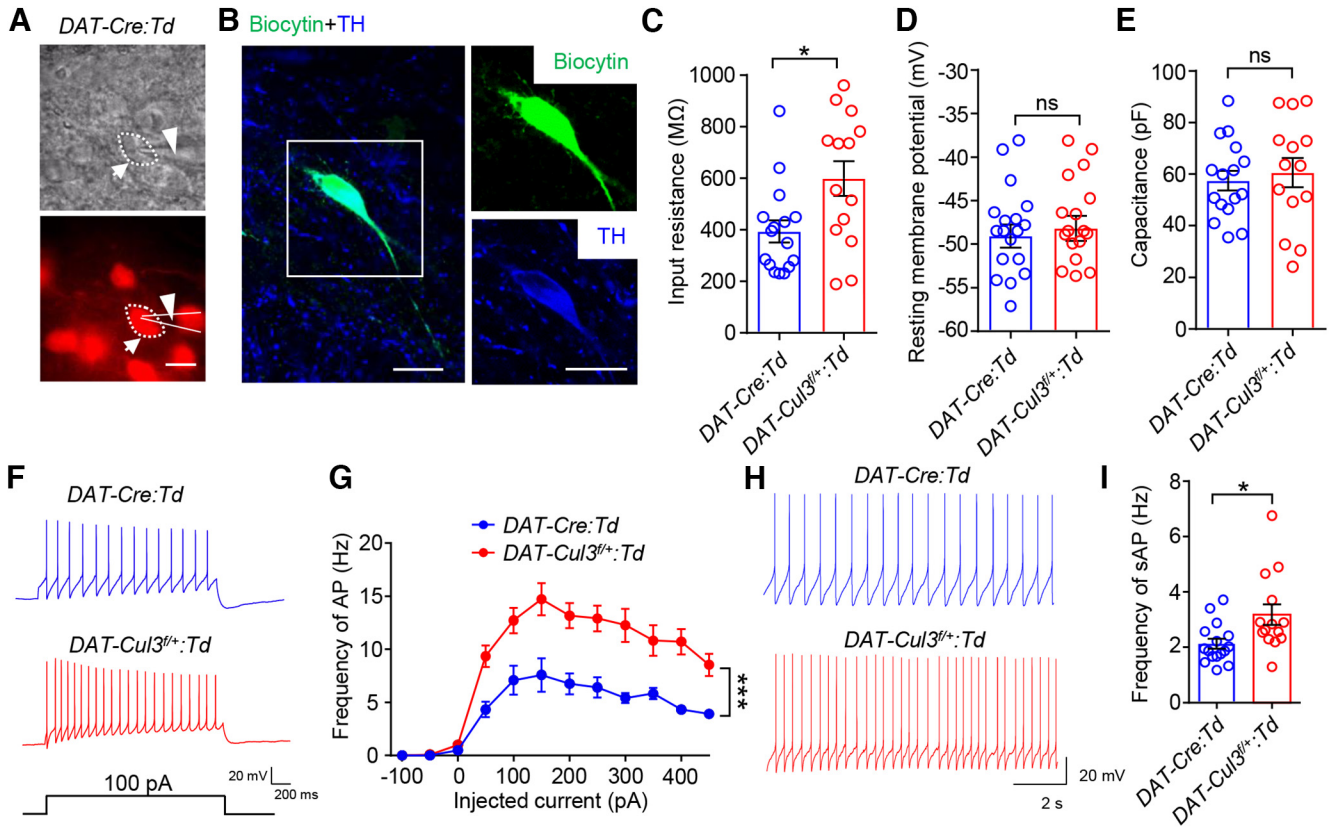

Figure 9. Increased VTA DA neuron excitability in *DAT-Cul3*$^{f/+}$ mice. ***A***, Image of a patched VTA DA neuron in a brain slice and the electrode. Top, Bright field image. Bottom, Fluorescent image for the same field. Red signal indicates tdTomato (Td). Scale bar, 20 μm. ***B***, Verification of recorded DA neurons by *post hoc* immunostaining toward injected biocytin using Alexa-488 conjugated streptavidin. Left, Confocal image of a biocytin-filled DA neuron (green) and TH staining (blue). Right, Enlarged image for biocytin (top) and TH (bottom) for the inset. Scale bar, 20 μm. ***C***, Increased membrane resistance of *DAT-Cul3*$^{f/+}$*:Td* VTA DA neuron. $n = 16$ neurons, 4 mice for *DAT-Cre:Td* group; $n = 14$ neurons, 4 mice for *DAT-Cul3*$^{f/+}$*:Td* group; $p = 0.0183$, $t_{(22.4)} = 2.545$; unpaired *t* test. ***D***, Comparable resting membrane potentials of VTA DA neurons. $n = 16$ neurons, 4 mice for *DAT-Cre:Td* group; $n = 14$ neurons, 4 mice for *DAT-Cul3*$^{f/+}$*:Td* group; *DAT-Cre:Td* (-48.63 ± 1.5 mV) versus *DAT-Cul3*$^{f/+}$*:Td* (-48.03 ± 1.8 mV), $p = 0.8014$, $t_{(26.39)} = 0.2541$; unpaired *t* test. ***E***, Similar capacitance. $n = 16$ neurons, 4 mice for *DAT-Cre:Td* group; $n = 14$ neurons, 4 mice for *DAT-Cul3*$^{f/+}$*:Td* group; $p = 0.6077$, $t_{(21.33)} = 0.5211$; unpaired *t* test. ***F***, Representative traces of spikes evoked by injection of depolarizing currents. ***G***, Increased firing rate evoked by current injection of *DAT-Cul3*$^{f/+}$*:Td* VTA DA neuron. Firing rate was plotted against increasing currents. $n = 12$ neurons, 4 mice for *DAT-Cre:Td* group; $n = 11$ neurons, 4 mice for *DAT-Cul3*$^{f/+}$*:Td* group; $p < 0.0001$, $F_{(genotype)(1,21)} = 33.52$; two-way ANOVA. ***H***, Representative traces of spontaneous spikes. ***I***, Increased frequency of spontaneous firing of APs of *DAT-Cul3*$^{f/+}$*:Td* VTA DA neuron. $n = 16$ neurons, 4 mice for *DAT-Cre:Td* group; $n = 14$ neurons, 4 mice for *DAT-Cul3*$^{f/+}$*:Td* group; $p = 0.0203$, $t_{(18.77)} = 2.536$; unpaired *t* test. Data are mean ± SEM. *$p < 0.05$.

social deficits and anxiety-like behavior as a result of increased neuronal excitability, glutamatergic transmission, and increased E/I ratio (Dong et al., 2020). Others have reported that loss of *Cul3* in PFC pyramidal neurons impaired the function of NMDA receptors and social interaction in mice, whereas decreased neuronal excitability and stereotypic behaviors were linked to the loss of *Cul3* in striatal medium spiny neurons (Rapanelli et al., 2021). Moreover, mice with *Cul3* loss in forebrain excitatory neurons or cholinergic neurons exhibited deficits in social interaction and sensorimotor gating (Rapanelli et al., 2021, 2023). In heterogeneous mice with DA-specific *Cul3* deletion, gross neuroanatomy of the brain was similar to control animals (Fig. 2), and neurogenesis and morphology of midbrain DA neurons were not impaired (Figs. 3, 8). Heterogeneous CUL3-deficient mice presented increased locomotor activity, impaired working memory, and decreased sensorimotor gating (Fig. 4) caused by increased DA neuronal excitability (Figs. 9, 10). Previous observations and our study imply an important role for CUL3 in controlling neuronal excitability across different types of neurons and brain regions.

Proteomic analyses have been performed to uncover differentially expressed proteins in brain tissues from mice with forebrain-specific *Cul3* deficiency (Rapanelli et al., 2021), projection neuron-selective *Cul3* deficiency (Dong et al., 2020), and mice with constitutive *Cul3* haploinsufficiency (Morandell et al., 2021). Interestingly, HCN2 is not among the significantly changed proteins in these studies. In addition to the discrepancies in the time points of the analyses, one possible explanation is that CUL3 interacts with different substrates in response to distinct pathways or protein expression profiles in different types of neurons. The specific substrates recognized by CUL3 can depend on factors, such as local protein expression levels, cell type-specific signaling, such as post-translational modifications, and the presence of specific adaptor proteins that interact with its substrate (Lydeard et al., 2013). As a scaffold to assemble Cullin-RING E3 ubiquitin ligase complex, CUL3 binds to BTB protein, a substrate recognition adaptor (Furukawa et al., 2003; Xu et al., 2003; Pintard et al., 2004). Over 100 BTB proteins contain the structural basis to bind CUL3 (Zhuang et al., 2009), implying the broad and diverse substrate spectrum of CUL3 (Wang et al., 2020).

DA signaling plays a crucial role in regulating various behaviors, such as locomotion, sensorimotor gating, and cognitive functions in human and rodent animal models (Iversen and Iversen, 2007). Overabundant DA signaling has been linked to increased locomotion (Pijnenburg and van Rossum, 1973;

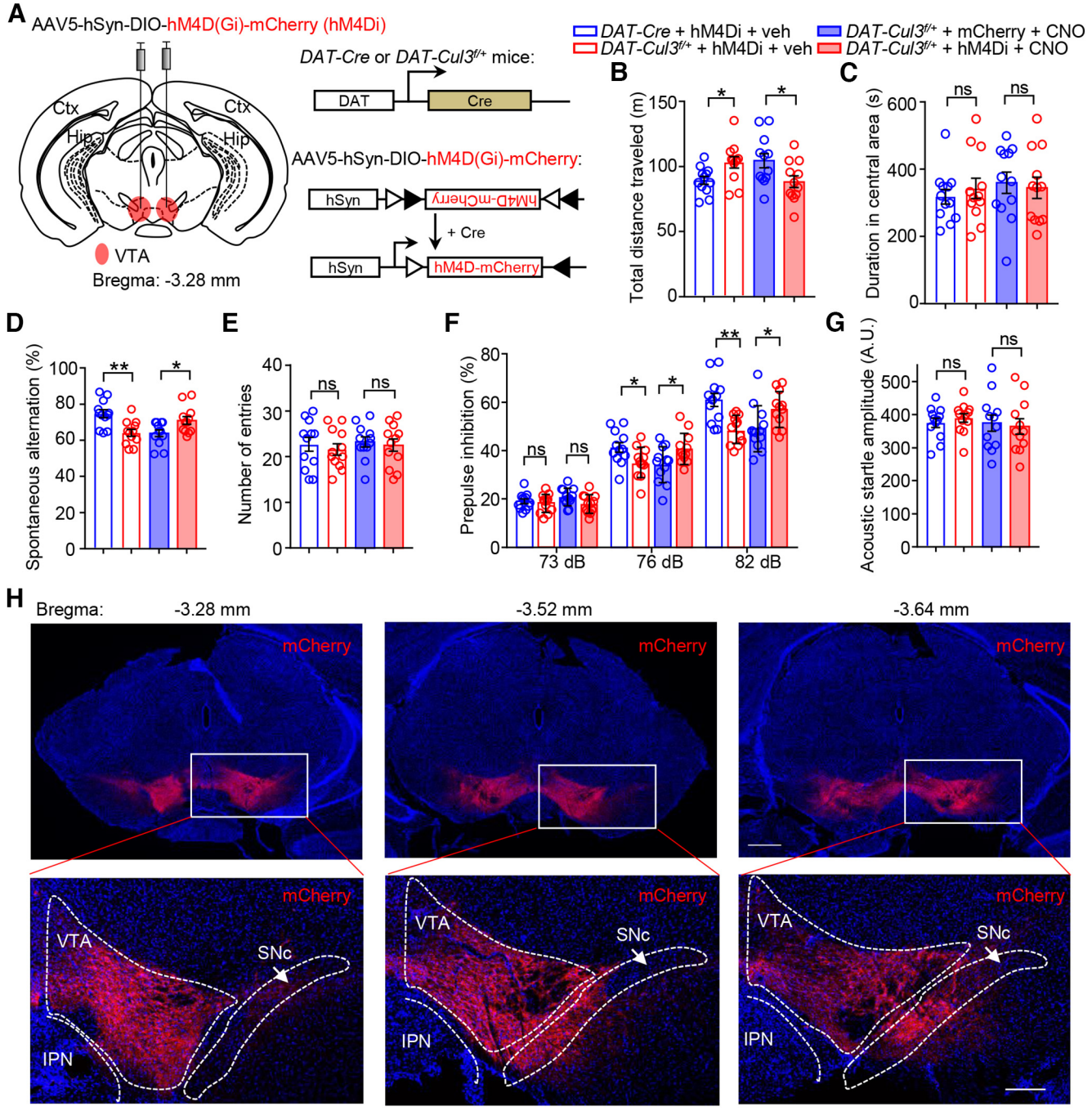

Figure 10. Attenuated hyperdopaminergic behaviors in *DAT-Cul3*$^{f/+}$ mice by chemogenetic inhibition of midbrain DA neurons. ***A***, Schematic diagram represents injection of AAV5-SunDIO-hM4D(Gi)-mCherry virus (hM4Di) into VTA in *DAT-Cre* or *DAT-Cul3*$^{f/+}$ mouse (left) and experimental approach for Cre-dependent expression of hM4Di-mCherry (right). AAV5-DIO-mCherry (mCherry) virus was injected as control. ***B***, Decreased distance traveled by hM4Di-injected *DAT-Cul3*$^{f/+}$ mice in the open field test after CNO injection (2 mg/kg, i.p.). $n = 12$ mice for all groups; for *DAT-Cre* + hM4Di + veh versus *DAT-Cul3*$^{f/+}$ + hM4Di + veh, $p = 0.0177$; *DAT-Cul3*$^{f/+}$ + mCherry + CNO versus *DAT-Cul3*$^{f/+}$ + hM4Di + CNO, $p = 0.0302$; unpaired *t* test. ***C***, Comparable time spent in the center in the open field after CNO injection. $n = 12$ mice for all groups; for *DAT-Cre* + hM4Di + veh versus *DAT-Cul3*$^{f/+}$ + hM4Di + veh, $p = 0.509$; *DAT-Cul3*$^{f/+}$ + mCherry + CNO versus *DAT-Cul3*$^{f/+}$ + hM4Di + CNO, $p = 0.7284$; unpaired *t* test. ***D***, Increased spontaneous alternation in hM4Di-injected *DAT-Cul3*$^{f/+}$ mice in Y-maze test after CNO injection. $n = 12$ mice for all groups; for *DAT-Cre* + hM4Di + veh versus *DAT-Cul3*$^{f/+}$ + hM4Di + veh, $p = 0.0015$; *DAT-Cul3*$^{f/+}$ + mCherry + CNO versus *DAT-Cul3*$^{f/+}$ + hM4Di + CNO, $p = 0.0219$; unpaired *t* test. ***E***, Comparable total number of entries in Y-maze after CNO injection. $n = 12$ mice for all groups; for *DAT-Cre* + hM4Di + veh versus *DAT-Cul3*$^{f/+}$ + hM4Di + veh, $p = 0.5886$; *DAT-Cul3*$^{f/+}$ + mCherry + CNO versus *DAT-Cul3*$^{f/+}$ + hM4Di + CNO, $p = 0.6722$; unpaired *t* test. ***F***, Restored PPI in hM4Di-injected *DAT-Cul3*$^{f/+}$ mice after CNO injection. $n = 12$ mice for all groups. For 73 dB, *DAT-Cre* + hM4Di + veh versus *DAT-Cul3*$^{f/+}$ + hM4Di + veh, $p = 0.5555$; *DAT-Cul3*$^{f/+}$ + mCherry + CNO versus *DAT-Cul3*$^{f/+}$ + hM4Di + CNO, $p = 0.0708$. For 76 dB, *DAT-Cre* + hM4Di + veh versus *DAT-Cul3*$^{f/+}$ + hM4Di + veh, $p = 0.03$; *DAT-Cul3*$^{f/+}$ + mCherry + CNO versus *DAT-Cul3*$^{f/+}$ + hM4Di + CNO, $p = 0.0310$. For 82 dB, *DAT-Cre* + hM4Di + veh versus *DAT-Cul3*$^{f/+}$ + hM4Di + veh, $p = 0.0013$; *DAT-Cul3*$^{f/+}$ + mCherry + CNO versus *DAT-Cul3*$^{f/+}$ + hM4Di + CNO, $p = 0.0342$; unpaired *t* test. ***G***, No impact on acoustic startle response by CNO for indicated groups. $n = 12$ mice for all groups; for *DAT-Cre* + hM4Di + veh versus *DAT-Cul3*$^{f/+}$ + hM4Di + veh, $p = 0.4624$; *DAT-Cul3*$^{f/+}$ + mCherry + CNO versus *DAT-Cul3*$^{f/+}$ + hM4Di + CNO, $p = 0.7720$; unpaired *t* test. ***H***, *Post hoc* staining to confirm the expression of the injected AAV5-DIO-hM4Di-mCherry virus. Top, Representative images of Cre-dependent expression of hM4Di-mCherry in *DAT-Cul3*$^{f/+}$ mouse in the midbrain. The coronal section of the midbrain was stained with mCherry antibody (visualized by AlexaFluor-594, red) and DAPI (blue). Scale bar, 500 μm. Bottom, Higher magnification of the insets in top panels. Scale bar, 200 μm. IPN, interpeduncular nucleus. Data are mean ± SEM. *$p < 0.05$. **$p < 0.01$.

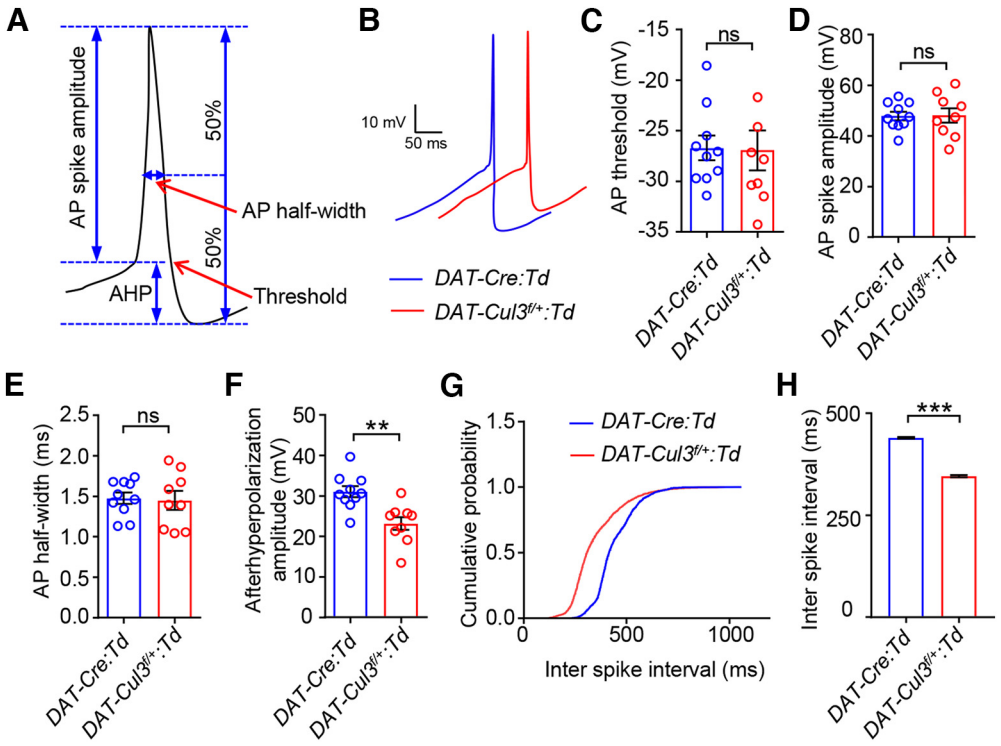

Figure 11. Decreased AHP amplitude in *DAT-Cul3*$^{f/+}$ VTA DA neuron. ***A***, Schematic diagram represents single AP recording. ***B***, Enlarged trace for a single AP from VTA DA neurons of indicated genotypes. ***C***, Comparable threshold for AP firing. $n = 10$ neurons, 4 mice for *DAT-Cre:Td* group; $n = 9$ neurons, 4 mice for *DAT-Cul3*$^{f/+}$*:Td* group; $p = 0.9300$, $t_{(13.55)} = 0.0895$; unpaired *t* test. ***D***, Similar spike amplitude of APs. $n = 10$ neurons, 4 mice for *DAT-Cre:Td* group; $n = 9$ neurons, 4 mice for *DAT-Cul3*$^{f/+}$*:Td* group; $p = 0.9472$, $t_{(13.09)} = 0.0676$; unpaired *t* test. ***E***, Similar half-width of APs. $n = 10$ neurons, 4 mice for *DAT-Cre:Td* group; $n = 9$ neurons, 4 mice for *DAT-Cul3*$^{f/+}$*:Td* group; $p = 0.8382$, $t_{(13.4)} = 0.2082$; unpaired *t* test. ***F***, Decreased AHP. $n = 10$ neurons, 4 mice for *DAT-Cre:Td* group; $n = 9$ neurons, 4 mice for *DAT-Cul3*$^{f/+}$*:Td* group; $p = 0.0021$, $t_{(16.09)} = 3.657$; unpaired *t* test. ***G***, ***H***, Decreased interspike interval (ISI). ***G***, Accumulative curve for the probability distribution of ISI, $p < 0.0001$, Kolmogorov–Smirnov test. ***H***, *DAT-Cre:Td* (440.3 ± 2.0 ms) versus *DAT-Cul3*$^{f/+}$*:Td* (346.5 ± 2.4 ms), $p < 0.0001$, $U = 1637985$; Mann Whitney test. $n = 2472$ events, 4 mice for *DAT-Cre:Td* group; $n = 2761$ events, 4 mice for *DAT-Cul3*$^{f/+}$*:Td* group. Data are mean ± SEM. $^{**}p < 0.01$. $^{***}p < 0.001$.

Gainetdinov et al., 1999). It has been indicated that working memory function has an inverted U-shaped relationship with DA, and excessive DA signaling has been implicated in disruptions to cognitive function (Vijayraghavan et al., 2007; Cools and D'Esposito, 2011). In addition, surplus DA transmission can impair sensorimotor gating, the ability of the brain to filter out irrelevant stimuli (Mansbach et al., 1988; Swerdlow et al., 1990b; J. Zhang et al., 2000; Ralph et al., 2001). We found that mice with CUL3 deficiency in DA neurons, especially in VTA DA neurons, exhibited abnormal behaviors that have been linked to hyperactive DA signaling, including increased spontaneous locomotion, impaired working memory performance in Y-maze, PPI deficits, and increased response to cocaine (Figs. 4-6). Moreover, DA signaling was enhanced in the NAc of CUL3-deficient mice (Fig. 7*B*,*C*). Accordingly, the DA-related behavioral deficits were mitigated by inhibition of DA neuron excitability via a chemogenetic approach (Fig. 10). Our findings suggest that the excessive activity of the DA pathway may be a potential cause for phenotypes of CUL3 deficiency.

Persistent upregulation of DA signaling may cause homeostatic or allostatic adaptation in downstream functions. Striatal D1DR and D2DR are reduced in DAT KO mice or mice given methamphetamine, likely because of excessive extracellular DA (McCabe et al., 1987; Giros et al., 1996). Activation of DA receptors could increase the internalization of D1DR and D2DR (Dumartin et al., 1998; Sun et al., 2003). In addition to DA receptor downregulation, enhanced DA activity could attenuate receptor sensitivity or induce desensitization by uncoupling DA receptors from signaling transduction (Barton et al., 1991; Ng et al., 1995; Cho et al., 2006). Whether these adaptation events occur in CUL3-deficient mice remains unclear. NAc D2DR levels were similar between CUL3-deficient mice and control mice (despite a trend of reduction that was not statistically significant) (Fig. 7*B*,*C*). It would be interesting to investigate whether and how DA signaling events homeostatically adapt to high DA activity in CUL3-deficient mice.

We showed that systemic administration of haloperidol alleviated behavioral abnormalities, including hyperactivity, working memory deficits, and decreased sensorimotor gating in CUL3-deficient animals (Fig. 10*B*-*G*). These results suggest the involvement of D2DR in CUL3 deficiency-caused abnormality. However, underlying mechanisms warrant further studies. The expression of D1DR and D2DR has been studied using many techniques, such as ISH, immunostaining (including immuno-EM), genetic labeling in D2DR-Cre/reporter mice, and most recently, single-cell RNA-sequencing analysis. Evidently, both are widely expressed in the brain, including regions, such as the cortex, hippocampus, amygdala, and striatum (Levey et al., 1993; Hersch et al., 1995; Le Moine and Bloch, 1995; Santana et al., 2009; Puighermanal et al., 2015; Dilly et al., 2022). Cell types that express D2DRs include pyramidal neurons, interneurons, and medium spiny neurons (Le Moine and Gaspar, 1998; Gee et al., 2012; Ho et al., 2018; Khlghatyan et al., 2019). Postsynaptic D2DR activation has been shown to reduce N-type Ca^{2+} currents in neostriatal cholinergic interneurons, alter striatal output neurons to enable the psychomotor effects of cocaine, and modulate striatal glutamatergic signaling in striatal medium spiny neurons (Yan et al., 1997). Haloperidol could

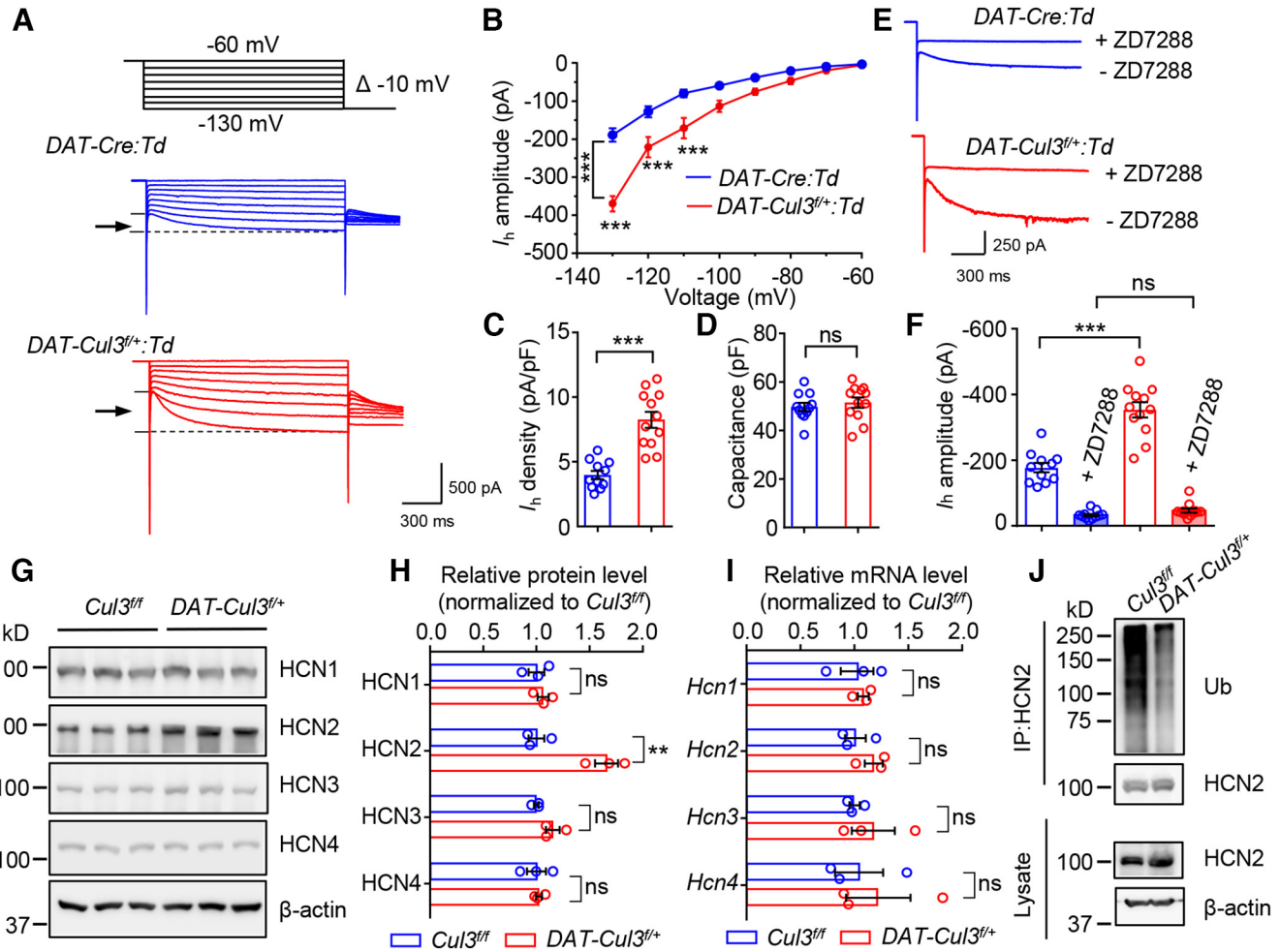

Figure 12. Increased function and expression of HCN2 channel in *DAT-Cul3*$^{f/+}$ mice. ***A***, Representative traces of I_h. ***B***, Increased amplitude of I_h in *DAT-Cul3*$^{f/+}$*:Td* VTA DA neurons. $n = 11$ neurons, 4 mice for *DAT-Cre:Td* group; $n = 12$ neurons, 4 mice for *DAT-Cul3*$^{f/+}$*:Td* group; $p = 0.0001$, $F_{(genotype)(1,21)} = 21.71$; two-way ANOVA followed by Bonferroni's *post hoc* test. ***C***, Increased density of I_h in *DAT-Cul3*$^{f/+}$*:Td* DA neurons. $n = 11$ neurons, 4 mice for *DAT-Cre:Td* group; $n = 12$ neurons, 4 mice for *DAT-Cul3*$^{f/+}$*:Td* group; $p < 0.0001$, $t_{(16.64)} = 6.103$; unpaired *t* test. ***D***, Comparable capacitance. $n = 11$ neurons, 4 mice for *DAT-Cre:Td* group; $n = 12$ neurons, 4 mice for *DAT-Cul3*$^{f/+}$*:Td* group; $p = 0.52$, $t_{(20.69)} = 0.6545$; unpaired *t* test. ***E***, Representative traces of I_h in the presence of HCN channel inhibitor ZD7288. ***F***, Similar amplitude of I_h in the presence of ZD7288. $n = 11$ neurons, 4 mice for *DAT-Cre:Td* group; $n = 12$ neurons, 4 mice for *DAT-Cul3*$^{f/+}$*:Td* group; *DAT-Cre:Td* versus *DAT-Cul3*$^{f/+}$*:Td*, $p < 0.0001$, $t_{(18.21)} = 6.408$; *DAT-Cre:Td* + ZD7288 versus *DAT-Cul3*$^{f/+}$*:Td* + ZD7288, $p = 0.0801$, $t_{(18.19)} = 1.854$; unpaired *t* test. ***G***, Increased levels of HCN2 protein in VTA/SNc of P60 *DAT-Cul3*$^{f/+}$ mice compared with control mice. ***H***, Quantification of data in ***G***. $n = 3$ mice for each genotype; for HCN1, $p = 0.5248$, $t_{(4)} = 0.6960$; for HCN2, $p = 0.0072$, $t_{(4)} = 5.066$; for HCN3, $p = 0.0873$, $t_{(4)} = 2.253$; for HCN4, $p = 0.8166$, $t_{(4)} = 0.2476$; unpaired *t* test. ***I***, Unchanged mRNA levels of *Hcn1-4* in VTA/SNc of *DAT-Cul3*$^{f/+}$ mice. $n = 3$ mice per group; for *Hcn1*, $p = 0.7356$, $t_{(4)} = 0.3621$; for *Hcn2*, $p = 0.2533$, $t_{(4)} = 1.333$; for *Hcn3*, $p = 0.4457$, $t_{(4)} = 0.845$; for *Hcn4*, $p = 0.6551$, $t_{(4)} = 0.4818$; unpaired *t* test. ***J***, Decreased ubiquitination of HCN2 in VTA/SNc of *DAT-Cul3*$^{f/+}$ mice. Data are mean ± SEM. $^{**}p < 0.01$. $^{***}p < 0.001$.

hinder the activation of downstream postsynaptic D2DR and mitigate the impact of hyperactive DA neurons in CUL3-deficient mice. On the other hand, D2DR on VTA DA cell bodies could serve as an inhibitory autoreceptor (Pucak and Grace, 1994; Ford, 2014). Its effect on DA neurons may depend on the activity state of DA neurons (Valenti et al., 2011). Furthermore, acutely, haloperidol increases VTA neuronal activity, but chronic administration decreases the activity of VTA neurons because of a depolarization block (Bunney et al., 1973; White and Wang, 1983; Grace and Bunney, 1986; Lane and Blaha, 1987). Which of the above mechanisms is involved in ameliorating CUL3 deficiency-caused deficits remains unclear.

HCN channels have been implicated in psychiatric and neurologic disorders (Benes et al., 2008; Schizophrenia Working Group of the Psychiatric Genomics Consortium, 2014; Greenwood et al., 2019). In midbrain DA neurons, HCN channels regulate the amplitude and duration of AHP that follows APs (Neuhoff et al., 2002; Okamoto et al., 2006; Lammel et al., 2008; Wanat et al., 2008). An increase in the HCN channel has been shown to reduce AHP and elevate AP firing in VTA DA neurons (Chu and Zhen, 2010; Santos-Vera et al., 2013; Friedman et al., 2014; Zhong et al., 2017). Increased amplitude of HCN-mediated I_h (Fig. 12*A*,*B*) and protein levels of HCN2 (Fig. 12*G*,*H*) were observed in CUL3-deficient mice. In contrast, the mRNA levels of *Hcn2* did not change (Fig. 12*I*), suggesting a post-transcriptional mechanism. Further biochemical experiments showed elevated poly-ubiquitination of HCN2 in VTA/SNc of CUL3-deficient mice (Fig. 12*J*). These data imply that HCN2 is a target of CUL3 in DA neurons and increased HCN2 protein enhances excitability of CUL3-deficient VTA DA neurons.

To summarize, using a cell type-specific KO mouse model combined with cell type- and region-specific viral approaches, this study uncovers the role of CUL3 in DA neurons and advances our knowledge of the pathologic mechanisms behind *Cul3* mutations and deficiencies in SZ and ASD.

References

Abi-Dargham A, Rodenhiser J, Printz D, Zea-Ponce Y, Gil R, Kegeles LS, Weiss R, Cooper TB, Mann JJ, Van Heertum RL, Gorman JM, Laruelle M (2000) Increased baseline occupancy of D2 receptors by dopamine in schizophrenia. Proc Natl Acad Sci USA 97:8104–8109.

Accili EA, Proenza C, Baruscotti M, DiFrancesco D (2002) From funny current to HCN channels: 20 years of excitation. News Physiol Sci 17:32–37.

Amar M, Pramod AB, Yu NK, Herrera VM, Qiu LR, Moran-Losada P, Zhang P, Trujillo CA, Ellegood J, Urresti J, Chau K, Diedrich J, Chen J, Gutierrez J, Sebat J, Ramanathan D, Lerch JP, Yates JR, Muotri AR, Iakoucheva LM (2021) Autism-linked Cullin3 germline haploinsufficiency impacts cytoskeletal dynamics and cortical neurogenesis through RhoA signaling. Mol Psychiatry 26:3586–3613.

Andérica-Romero AC, González-Herrera IG, Santamaría A, Pedraza-Chaverri J (2013) Cullin 3 as a novel target in diverse pathologies. Redox Biol 1:366–372.

Anderson GM (1994) Studies on the neurochemistry of autism. In: The neurobiology of autism (Bauman ML KT, ed), pp 227–242. Baltimore: Johns Hopkins UP.

Anderson LT, Campbell M, Grega DM, Perry R, Small AM, Green WH (1984) Haloperidol in the treatment of infantile autism: effects on learning and behavioral symptoms. Am J Psychiatry 141:1195–1202.

Anzalone A, Lizardi-Ortiz JE, Ramos M, De Mei C, Hopf FW, Iaccarino C, Halbout B, Jacobsen J, Kinoshita C, Welter M, Caron MG, Bonci A, Sulzer D, Borrelli E (2012) Dual control of dopamine synthesis and release by presynaptic and postsynaptic dopamine D2 receptors. J Neurosci 32:9023–9034.

Armbruster BN, Li X, Pausch MH, Herlitze S, Roth BL (2007) Evolving the lock to fit the key to create a family of G protein-coupled receptors potently activated by an inert ligand. Proc Natl Acad Sci USA 104:5163–5168.

Bäckman CM, Malik N, Zhang Y, Shan L, Grinberg A, Hoffer BJ, Westphal H, Tomac AC (2006) Characterization of a mouse strain expressing Cre recombinase from the 3′ untranslated region of the dopamine transporter locus. Genesis 44:383–390.

Barbeau A, Sourkes T, Murphy G (1962) Les catecholamines dans la maladie de parkinson. In: Monoamines et systeme nerveux central (de Ajuriaguerra J, ed). Geneva: Georg.

Barton AC, Black LE, Sibley DR (1991) Agonist-induced desensitization of D2 dopamine receptors in human Y-79 retinoblastoma cells. Mol Pharmacol 39:650–658.

Beaulieu JM, Gainetdinov RR, Caron MG (2007) The Akt-GSK-3 signaling cascade in the actions of dopamine. Trends Pharmacol Sci 28:166–172.

Bello EP, Mateo Y, Gelman DM, Noaín D, Shin JH, Low MJ, Alvarez VA, Lovinger DM, Rubinstein M (2011) Cocaine supersensitivity and enhanced motivation for reward in mice lacking dopamine D2 autoreceptors. Nat Neurosci 14:1033–1038.

Benes FM, Lim B, Matzilevich D, Subburaju S, Walsh JP (2008) Circuitry-based gene expression profiles in GABA cells of the trisynaptic pathway in schizophrenics versus bipolars. Proc Natl Acad Sci USA 105:20935–20940.

Bird ED, Spokes EG, Iversen LL (1979) Increased dopamine concentration in limbic areas of brain from patients dying with schizophrenia. Brain 102:347–360.

Bunney BS, Walters JR, Roth RH, Aghajanian GK (1973) Dopaminergic neurons: effect of antipsychotic drugs and amphetamine on single cell activity. J Pharmacol Exp Ther 185:560–571.

Chau V, Tobias JW, Bachmair A, Marriott D, Ecker DJ, Gonda DK, Varshavsky A (1989) A multiubiquitin chain is confined to specific lysine in a targeted short-lived protein. Science 243:1576–1583.

Cho DI, Beom S, Van Tol HH, Caron MG, Kim KM (2006) Characterization of the desensitization properties of five dopamine receptor subtypes and alternatively spliced variants of dopamine D2 and D4 receptors. Biochem Biophys Res Commun 350:634–640.

Chu H, Zhen X (2010) Hyperpolarization-activated, cyclic nucleotide-gated (HCN) channels in the regulation of midbrain dopamine systems. Acta Pharmacol Sin 31:1036–1043.

Cools R, D'Esposito M (2011) Inverted-U-shaped dopamine actions on human working memory and cognitive control. Biol Psychiatry 69:e113-25.

De Rubeis S, et al., UK10K Consortium (2014) Synaptic, transcriptional and chromatin genes disrupted in autism. Nature 515:209–215.

Deshaies RJ (1999) SCF and Cullin/Ring H2-based ubiquitin ligases. Annu Rev Cell Dev Biol 15:435–467.

Dilly GA, Kittleman CW, Kerr TM, Messing RO, Mayfield RD (2022) Cell type specific changes in PKC-delta neurons of the central amygdala during alcohol withdrawal. Transl Psychiatry 12:289.

Djagaeva I, Doronkin S (2009) COP9 limits dendritic branching via Cullin3-dependent degradation of the actin-crosslinking BTB-domain protein Kelch. PLoS One 4:e7598.

Dong Z, Chen W, Chen C, Wang H, Cui W, Tan Z, Robinson H, Gao N, Luo B, Zhang L, Zhao K, Xiong WC, Mei L (2020) CUL3 deficiency causes social deficits and anxiety-like behaviors by impairing excitation-inhibition balance through the promotion of Cap-dependent translation. Neuron 105:475–490.e476.

Dumartin B, Caillé I, Gonon F, Bloch B (1998) Internalization of D1 dopamine receptor in striatal neurons in vivo as evidence of activation by dopamine agonists. J Neurosci 18:1650–1661.

Ehringer H, Hornykiewicz O (1960) Verteilung Von Noradrenalin Und Dopamin (3-Hydroxytyramin) Im Gehirn Des Menschen Und Ihr Verhalten Bei Erkrankungen Des Extrapyramidalen Systems. Klin Wochenschr 38:1236–1239.

Escamilla CO, Filonova I, Walker AK, Xuan ZX, Holehonnur R, Espinosa F, Liu S, Thyme SB, López-García IA, Mendoza DB, Usui N, Ellegood J, Eisch AJ, Konopka G, Lerch JP, Schier AF, Speed HE, Powell CM (2017) Kctd13 deletion reduces synaptic transmission via increased RhoA. Nature 551:227–231.

Farde L, Wiesel FA, Halldin C, Sedvall G (1988) Central D2-dopamine receptor occupancy in schizophrenic patients treated with antipsychotic drugs. Arch Gen Psychiatry 45:71–76.

Ford CP (2014) The role of D2-autoreceptors in regulating dopamine neuron activity and transmission. Neuroscience 282:13–22.

Friedman AK, Walsh JJ, Juarez B, Ku SM, Chaudhury D, Wang J, Li X, Dietz DM, Pan N, Vialou VF, Neve RL, Yue Z, Han MH (2014) Enhancing depression mechanisms in midbrain dopamine neurons achieves homeostatic resilience. Science 344:313–319.

Fromer M, et al. (2014) De novo mutations in schizophrenia implicate synaptic networks. Nature 506:179–184.

Furukawa M, He YJ, Borchers C, Xiong Y (2003) Targeting of protein ubiquitination by BTB–Cullin 3–Roc1 ubiquitin ligases. Nat Cell Biol 5:1001–1007.

Gainetdinov RR, Jones SR, Caron MG (1999) Functional hyperdopaminergia in dopamine transporter knock-out mice. Biol Psychiatry 46:303–311.

Gee S, Ellwood I, Patel T, Luongo F, Deisseroth K, Sohal VS (2012) Synaptic activity unmasks dopamine D2 receptor modulation of a specific class of layer V pyramidal neurons in prefrontal cortex. J Neurosci 32:4959–4971.

Geyer MA, Swerdlow NR (1998) Measurement of startle response, prepulse inhibition, and habituation. Curr Protoc Neurosci 3:1-8.

Geyer MA, Swerdlow NR, Mansbach RS, Braff DL (1990) Startle response models of sensorimotor gating and habituation deficits in schizophrenia. Brain Res Bull 25:485–498.

Girault JA, Greengard P (2004) The neurobiology of dopamine signaling. Arch Neurol 61:641–644.

Giros B, Jaber M, Jones SR, Wightman RM, Caron MG (1996) Hyperlocomotion and indifference to cocaine and amphetamine in mice lacking the dopamine transporter. Nature 379:606–612.

Grace AA, Bunney BS (1986) Induction of depolarization block in midbrain dopamine neurons by repeated administration of haloperidol: analysis using in vivo intracellular recording. J Pharmacol Exp Ther 238:1092–1100.

Grace AA, Onn SP (1989) Morphology and electrophysiological properties of immunocytochemically identified rat dopamine neurons recorded in vitro. J Neurosci 9:3463–3481.

Greenwood TA, et al. (2019) Genome-wide Association of Endophenotypes for Schizophrenia from the Consortium on the Genetics of Schizophrenia (COGS) Study. JAMA Psychiatry 76:1274–1284.

Harris NC, Constanti A (1995) Mechanism of block by ZD 7288 of the hyperpolarization-activated inward rectifying current in guinea pig substantia nigra neurons in vitro. J Neurophysiol 74:2366–2378.

Hersch SM, Ciliax BJ, Gutekunst CA, Rees HD, Heilman CJ, Yung KK, Bolam JP, Ince E, Yi H, Levey AI (1995) Electron microscopic analysis of D1 and D2 dopamine receptor proteins in the dorsal striatum and their synaptic relationships with motor corticostriatal afferents. J Neurosci 15:5222–5237.

Ho H, Both M, Siniard A, Sharma S, Notwell JH, Wallace M, Leone DP, Nguyen A, Zhao E, Lee H, Zwilling D, Thompson KR, Braithwaite SP, Huentelman M, Portmann T (2018) A guide to single-cell transcriptomics in adult rodent brain: the medium spiny neuron transcriptome revisited. Front Cell Neurosci 12:159.

Hoffman HS, Ison JR (1980) Reflex modification in the domain of startle: I. Some empirical findings and their implications for how the nervous system processes sensory input. Psychol Rev 87:175–189.

Iversen SD, Iversen LL (2007) Dopamine: 50 years in perspective. Trends Neurosci 30:188–193.

Kaspar JW, Niture SK, Jaiswal AK (2009) Nrf2: INrf2 (Keap1) signaling in oxidative stress. Free Radic Biol Med 47:1304–1309.

Khanzada NS, Butler MG, Manzardo AM (2017) GeneAnalytics pathway analysis and genetic overlap among autism spectrum disorder, bipolar disorder and schizophrenia. Int J Mol Sci 18:527.

Khlghatyan J, Quintana C, Parent M, Beaulieu JM (2019) High sensitivity mapping of cortical dopamine D2 receptor expressing neurons. Cereb Cortex 29:3813–3827.

Kikuma K, Li X, Perry S, Li Q, Goel P, Chen C, Kim D, Stavropoulos N, Dickman D (2019) Cul3 and insomniac are required for rapid ubiquitination of postsynaptic targets and retrograde homeostatic signaling. Nat Commun 10:2998.

Kish SJ, Shannak K, Hornykiewicz O (1988) Uneven pattern of dopamine loss in the striatum of patients with idiopathic Parkinson's disease: pathophysiologic and clinical implications. N Engl J Med 318:876–880.

Klein MO, Battagello DS, Cardoso AR, Hauser DN, Bittencourt JC, Correa RG (2019) Dopamine: functions, signaling, and association with neurological diseases. Cell Mol Neurobiol 39:31–59.

Krashes MJ, Koda S, Ye C, Rogan SC, Adams AC, Cusher DS, Maratos-Flier E, Roth BL, Lowell BB (2011) Rapid, reversible activation of AgRP neurons drives feeding behavior in mice. J Clin Invest 121:1424–1428.

Lacey MG, Mercuri NB, North RA (1989) Two cell types in rat substantia nigra zona compacta distinguished by membrane properties and the actions of dopamine and opioids. J Neurosci 9:1233–1241.

Lammel S, Hetzel A, Häckel O, Jones I, Liss B, Roeper J (2008) Unique properties of mesoprefrontal neurons within a dual mesocorticolimbic dopamine system. Neuron 57:760–773.

Lammel S, Ion DI, Roeper J, Malenka RC (2011) Projection-specific modulation of dopamine neuron synapses by aversive and rewarding stimuli. Neuron 70:855–862.

Lammel S, Steinberg EE, Földy C, Wall NR, Beier K, Luo L, Malenka RC (2015) Diversity of transgenic mouse models for selective targeting of midbrain dopamine neurons. Neuron 85:429–438.

Lane RF, Blaha CD (1987) Chronic haloperidol decreases dopamine release in striatum and nucleus accumbens in vivo: depolarization block as a possible mechanism of action. Brain Res Bull 18:135–138.

Le Moine C, Bloch B (1995) D1 and D2 dopamine receptor gene expression in the rat striatum: sensitive cRNA probes demonstrate prominent segregation of D1 and D2 mRNAs in distinct neuronal populations of the dorsal and ventral striatum. J Comp Neurol 355:418–426.

Le Moine C, Gaspar P (1998) Subpopulations of cortical GABAergic interneurons differ by their expression of D1 and D2 dopamine receptor subtypes. Brain Res Mol Brain Res 58:231–236.

Lee YR, Yuan WC, Ho HC, Chen CH, Shih HM, Chen RH (2010) The Cullin 3 substrate adaptor KLHL20 mediates DAPK ubiquitination to control interferon responses. EMBO J 29:1748–1761.

Levey AI, Hersch SM, Rye DB, Sunahara RK, Niznik HB, Kitt CA, Price DL, Maggio R, Brann MR, Ciliax BJ (1993) Localization of D1 and D2 dopamine receptors in brain with subtype-specific antibodies. Proc Natl Acad Sci USA 90:8861–8865.

Li L, Cao Y, Wu H, Ye X, Zhu Z, Xing G, Shen C, Barik A, Zhang B, Xie X, Zhi W, Gan L, Su H, Xiong WC, Mei L (2016) Enzymatic activity of the scaffold protein rapsyn for synapse formation. Neuron 92:1007–1019.

Lin MY, Lin YM, Kao TC, Chuang HH, Chen RH (2011) PDZ-RhoGEF ubiquitination by Cullin3-KLHL20 controls neurotrophin-induced neurite outgrowth. J Cell Biol 193:985–994.

Ludwig A, Zong X, Jeglitsch M, Hofmann F, Biel M (1998) A family of hyperpolarization-activated mammalian cation channels. Nature 393:587–591.

Lydeard JR, Schulman BA, Harper JW (2013) Building and remodelling Cullin–RING E3 ubiquitin ligases. EMBO Rep 14:1050–1061.

Mackay AV, Iversen LL, Rossor M, Spokes E, Bird E, Arregui A, Creese I, Snyder SH (1982) Increased brain dopamine and dopamine receptors in schizophrenia. Arch Gen Psychiatry 39:991–997.

Madisen L, Zwingman TA, Sunkin SM, Oh SW, Zariwala HA, Gu H, Ng LL, Palmiter RD, Hawrylycz MJ, Jones AR, Lein ES, Zeng H (2010) A robust and high-throughput Cre reporting and characterization system for the whole mouse brain. Nat Neurosci 13:133–140.

Mansbach RS, Geyer MA, Braff DL (1988) Dopaminergic stimulation disrupts sensorimotor gating in the rat. Psychopharmacology (Berl) 94:507–514.

McCabe RT, Hanson GR, Dawson TM, Wamsley JK, Gibb JW (1987) Methamphetamine-induced reduction in D1 and D2 dopamine receptors as evidenced by autoradiography: comparison with tyrosine hydroxylase activity. Neuroscience 23:253–261.

McCracken JT, et al., Research Units on Pediatric Psychopharmacology Autism Network (2002) Risperidone in children with autism and serious behavioral problems. N Engl J Med 347:314–321.

McDaid J, McElvain MA, Brodie MS (2008) Ethanol effects on dopaminergic ventral tegmental area neurons during block of Ih: involvement of barium-sensitive potassium currents. J Neurophysiol 100:1202–1210.

McEvoy JD, Kossatz U, Malek N, Singer JD (2007) Constitutive turnover of cyclin E by Cul3 maintains quiescence. Mol Cell Biol 27:3651–3666.

Meltzer HY, Matsubara S, Lee JC (1989) Classification of typical and atypical antipsychotic drugs on the basis of dopamine D-1, D-2 and serotonin2 pKi values. J Pharmacol Exp Ther 251:238–246.

Missale C, Nash SR, Robinson SW, Jaber M, Caron MG (1998) Dopamine receptors: from structure to function. Physiol Rev 78:189–225.

Monteggia LM, Eisch AJ, Tang MD, Kaczmarek LK, Nestler EJ (2000) Cloning and localization of the hyperpolarization-activated cyclic nucleotide-gated channel family in rat brain. Brain Res Mol Brain Res 81:129–139.

Morandell J, Schwarz LA, Basilico B, Tasciyan S, Dimchev G, Nicolas A, Sommer C, Kreuzinger C, Dotter CP, Knaus LS, Dobler Z, Cacci E, Schur FK, Danzl JG, Novarino G (2021) Cul3 regulates cytoskeleton protein homeostasis and cell migration during a critical window of brain development. Nat Commun 12:3058.

Neuhoff H, Neu A, Liss B, Roeper J (2002) Ih channels contribute to the different functional properties of identified dopaminergic subpopulations in the midbrain. J Neurosci 22:1290–1302.

Neve KA, Seamans JK, Trantham-Davidson H (2004) Dopamine receptor signaling. J Recept Signal Transduct Res 24:165–205.

Ng GY, Trogadis J, Stevens J, Bouvier M, O'Dowd BF, George SR (1995) Agonist-induced desensitization of dopamine D1 receptor-stimulated adenylyl cyclase activity is temporally and biochemically separated from D1 receptor internalization. Proc Natl Acad Sci USA 92:10157–10161.

Notomi T, Shigemoto R (2004) Immunohistochemical localization of Ih channel subunits, HCN1-4, in the rat brain. J Comp Neurol 471:241–276.

Nyberg S, Farde L, Eriksson L, Halldin C, Eriksson B (1993) 5-HT2 and D2 dopamine receptor occupancy in the living human brain: a PET study with risperidone. Psychopharmacology (Berl) 110:265–272.

Okamoto T, Harnett MT, Morikawa H (2006) Hyperpolarization-activated cation current (Ih) is an ethanol target in midbrain dopamine neurons of mice. J Neurophysiol 95:619–626.

Parker KE, Pedersen CE, Gomez AM, Spangler SM, Walicki MC, Feng SY, Stewart SL, Otis JM, Al-Hasani R, McCall JG, Sakers K, Bhatti DL, Copits BA, Gereau RW, Jhou T, Kash TJ, Dougherty JD, Stuber GD, Bruchas MR (2019) A paranigral VTA nociceptin circuit that constrains motivation for reward. Cell 178:653–671.e619.

Pavăl D (2017) A dopamine hypothesis of autism spectrum disorder. Dev Neurosci 39:355–360.

Pignatelli M, Bonci A (2015) Role of dopamine neurons in reward and aversion: a synaptic plasticity perspective. Neuron 86:1145–1157.

Pijnenburg AJ, van Rossum JM (1973) Stimulation of locomotor activity following injection of dopamine into the nucleus accumbens. J Pharm Pharmacol 25:1003–1005.

Pintard L, Willems A, Peter M (2004) Cullin-based ubiquitin ligases: cul3-BTB complexes join the family. EMBO J 23:1681–1687.

Pucak ML, Grace AA (1994) Evidence that systemically administered dopamine antagonists activate dopamine neuron firing primarily by blockade of somatodendritic autoreceptors. J Pharmacol Exp Ther 271:1181–1192.

Puighermanal E, Biever A, Espallergues J, Gangarossa G, De Bundel D, Valjent E (2015) drd2-cre:ribotag mouse line unravels the possible

diversity of dopamine d2 receptor-expressing cells of the dorsal mouse hippocampus. Hippocampus 25:858–875.
Ralph RJ, Paulus MP, Fumagalli F, Caron MG, Geyer MA (2001) Prepulse inhibition deficits and perseverative motor patterns in dopamine transporter knock-out mice: differential effects of D1 and D2 receptor antagonists. J Neurosci 21:305–313.
Rapanelli M, Tan T, Wang W, Wang X, Wang ZJ, Zhong P, Frick L, Qin L, Ma K, Qu J, Yan Z (2021) Behavioral, circuitry, and molecular aberrations by region-specific deficiency of the high-risk autism gene Cul3. Mol Psychiatry 26:1491–1504.
Rapanelli M, Wang W, Hurley E, Feltri ML, Pittenger C, Frick LR, Yan Z (2023) Cholinergic neurons in the basal forebrain are involved in behavioral abnormalities associated with Cul3 deficiency: role of prefrontal cortex projections in cognitive deficits. Transl Psychiatry 13:22.
Santana N, Mengod G, Artigas F (2009) Quantitative analysis of the expression of dopamine D1 and D2 receptors in pyramidal and GABAergic neurons of the rat prefrontal cortex. Cereb Cortex 19:849–860.
Santoro B, Liu DT, Yao H, Bartsch D, Kandel ER, Siegelbaum SA, Tibbs GR (1998) Identification of a gene encoding a hyperpolarization-activated pacemaker channel of brain. Cell 93:717–729.
Santoro B, Chen S, Luthi A, Pavlidis P, Shumyatsky GP, Tibbs GR, Siegelbaum SA (2000) Molecular and functional heterogeneity of hyperpolarization-activated pacemaker channels in the mouse CNS. J Neurosci 20:5264–5275.
Santos-Vera B, Vázquez-Torres R, Marrero HG, Acevedo JM, Arencibia-Albite F, Vélez-Hernández ME, Miranda JD, Jiménez-Rivera CA (2013) Cocaine sensitization increases Ih current channel subunit 2 (HCN2) protein expression in structures of the mesocorticolimbic system. J Mol Neurosci 50:234–245.
Schizophrenia Working Group of the Psychiatric Genomics Consortium (2014) Biological insights from 108 schizophrenia-associated genetic loci. Nature 511:421.
Seeman P, Chau-Wong M, Tedesco J, Wong K (1975) Brain receptors for antipsychotic drugs and dopamine: direct binding assays. Proc Natl Acad Sci USA 72:4376–4380.
Singer JD, Gurian-West M, Clurman B, Roberts JM (1999) Cullin-3 targets cyclin E for ubiquitination and controls S phase in mammalian cells. Genes Dev 13:2375–2387.
Slifstein M, van de Giessen E, Van Snellenberg J, Thompson JL, Narendran R, Gil R, Hackett E, Girgis R, Ojeil N, Moore H, D'Souza D, Malison RT, Huang Y, Lim K, Nabulsi N, Carson RE, Lieberman JA, Abi-Dargham A (2015) Deficits in prefrontal cortical and extrastriatal dopamine release in schizophrenia: a positron emission tomographic functional magnetic resonance imaging study. JAMA Psychiatry 72:316–324.
Sun W, Ginovart N, Ko F, Seeman P, Kapur S (2003) In vivo evidence for dopamine-mediated internalization of D2-receptors after amphetamine: differential findings with [^{3}H]raclopride versus [^{3}H]spiperone. Mol Pharmacol 63:456–462.
Swerdlow NR, Braff DL, Masten VL, Geyer MA (1990a) Schizophrenic-like sensorimotor gating abnormalities in rats following dopamine infusion into the nucleus accumbens. Psychopharmacology (Berl) 101:414–420.
Swerdlow NR, Mansbach RS, Geyer MA, Pulvirenti L, Koob GF, Braff DL (1990b) Amphetamine disruption of prepulse inhibition of acoustic startle is reversed by depletion of mesolimbic dopamine. Psychopharmacology (Berl) 100:413–416.
Swerdlow NR, Caine SB, Braff DL, Geyer MA (1992) The neural substrates of sensorimotor gating of the startle reflex: a review of recent findings and their implications. J Psychopharmacol 6:176–190.
Swerdlow NR, Braff DL, Geyer MA (2016) Sensorimotor gating of the startle reflex: what we said 25 years ago, what has happened since then, and what comes next. J Psychopharmacol 30:1072–1081.
Tan ZB, Robinson HL, Yin DM, Liu Y, Liu F, Wang HS, Lin TW, Xing GL, Gan L, Xiong WC, Mei L (2018) Dynamic ErbB4 activity in hippocampal-prefrontal synchrony and top-down attention in rodents. Neuron 98:380–393.e4.
Tritsch NX, Sabatini BL (2012) Dopaminergic modulation of synaptic transmission in cortex and striatum. Neuron 76:33–50.
Urban DJ, Roth BL (2015) DREADDs (designer receptors exclusively activated by designer drugs): chemogenetic tools with therapeutic utility. Annu Rev Pharmacol Toxicol 55:399–417.
Valenti O, Cifelli P, Gill KM, Grace AA (2011) Antipsychotic drugs rapidly induce dopamine neuron depolarization block in a developmental rat model of schizophrenia. J Neurosci 31:12330–12338.
Vandegrift BJ, Hilderbrand ER, Satta R, Tai R, He D, You C, Chen H, Xu P, Coles C, Brodie MS, Lasek AW (2020) Estrogen receptor α regulates ethanol excitation of ventral tegmental area neurons and binge drinking in female mice. J Neurosci 40:5196–5207.
Vijayraghavan S, Wang M, Birnbaum SG, Williams GV, Arnsten AF (2007) Inverted-U dopamine D1 receptor actions on prefrontal neurons engaged in working memory. Nat Neurosci 10:376–384.
Wahl-Schott C, Biel M (2009) HCN channels: structure, cellular regulation and physiological function. Cell Mol Life Sci 66:470–494.
Wanat MJ, Hopf FW, Stuber GD, Phillips PE, Bonci A (2008) Corticotropin-releasing factor increases mouse ventral tegmental area dopamine neuron firing through a protein kinase C-dependent enhancement of Ih. J Physiol 586:2157–2170.
Wang P, Song J, Ye D (2020) CRL3s: the BTB-CUL3-RING E3 ubiquitin ligases. In: Cullin-RING ligases and protein neddylation: biology and therapeutics (Sun Y, Wei W, Jin J, eds), pp 211–223. Singapore: Springer.
Weinstein JJ, Chohan MO, Slifstein M, Kegeles LS, Moore H, Abi-Dargham A (2017) Pathway-specific dopamine abnormalities in schizophrenia. Biol Psychiatry 81:31–42.
White FJ, Wang RY (1983) Differential effects of classical and atypical antipsychotic drugs on A9 and A10 dopamine neurons. Science 221:1054–1057.
Winterer G, Weinberger DR (2004) Genes, dopamine and cortical signal-to-noise ratio in schizophrenia. Trends Neurosci 27:683–690.
Xu L, Wei Y, Reboul J, Vaglio P, Shin TH, Vidal M, Elledge SJ, Harper JW (2003) BTB proteins are substrate-specific adaptors in an SCF-like modular ubiquitin ligase containing CUL-3. Nature 425:316–321.
Yan Z, Song WJ, Surmeier J (1997) D2 dopamine receptors reduce N-type Ca^{2+} currents in rat neostriatal cholinergic interneurons through a membrane-delimited, protein-kinase-C-insensitive pathway. J Neurophysiol 77:1003–1015.
Zhang H, Chen W, Tan Z, Zhang L, Dong Z, Cui W, Zhao K, Wang H, Jing H, Cao R, Kim C, Safar JG, Xiong WC, Mei L (2020) A role of low-density lipoprotein receptor-related protein 4 (LRP4) in astrocytic Aβ clearance. J Neurosci 40:5347–5361.
Zhang J, Forkstam C, Engel JA, Svensson L (2000) Role of dopamine in prepulse inhibition of acoustic startle. Psychopharmacology (Berl) 149:181–188.
Zhang TA, Placzek AN, Dani JA (2010) In vitro identification and electrophysiological characterization of dopamine neurons in the ventral tegmental area. Neuropharmacology 59:431–436.
Zhong P, Vickstrom CR, Liu X, Hu Y, Yu L, Yu HG, Liu Q (2017) HCN2 channels in the ventral tegmental area regulate behavioral responses to chronic stress. Elife 7:e32420.
Zhu H, Pleil KE, Urban DJ, Moy SS, Kash TL, Roth BL (2014) Chemogenetic inactivation of ventral hippocampal glutamatergic neurons disrupts consolidation of contextual fear memory. Neuropsychopharmacology 39:1880–1892.
Zhuang M, Calabrese MF, Liu J, Waddell MB, Nourse A, Hammel M, Miller DJ, Walden H, Duda DM, Seyedin SN, Hoggard T, Harper JW, White KP, Schulman BA (2009) Structures of SPOP-substrate complexes: insights into molecular architectures of BTB-Cul3 ubiquitin ligases. Mol Cell 36:39–50.